UNIVERSITY OF CALIFORNIA,
IRVINE

Fabrication and Characterization of Dye-Sensitized Solar Cells with Efficient Regeneration Between Oxidized Dyes and Reduced Redox Shuttle Species

THESIS

submitted in partial satisfaction of the requirements
for the degree of

MASTER OF SCIENCE

in Chemical and Biochemical Engineering

by

Nazila Farhang

Thesis Committee:
Assistant Professor Shane Ardo, Chair
Associate Professor Matthew D. Law
Chancellor's Professor Reginald M. Penner

2019

DEDICATION

To my mother, father, and sister for all the love, encouragement, and support they have provided me throughout my life.
In loving memory of my cousin, Kia Kermani. Sometimes memories of you sneak out of my eyes and roll down my cheeks.

TABLE OF CONTENTS

LIST OF FIGURES

LIST OF TABLES

ACKNOWLEDGMENTS

I am so, so grateful that I have had so many wonderful people that have made this dream of mine a reality. None of my successes in the graduate school could have been achieved without the mentorship and support of countless people in my life, including my family, all of my wonderful friends, great teachers and research mentors at UC Irvine.

I would first like to express the deepest appreciation to my advisor and committee chair, Dr. Shane Ardo who gave me the opportunity to work with him as a master's student. If it was not for his taking a chance on me, this future would have not been possible. Dr. Ardo's passion in his work has shown me that there are individuals who really work hard towards in developing new innovative renewable energy sources. During my time working with the Ardo's group, I have found that Dr. Ardo fosters a uniquely comfortable working environment, always ready to help if a particular problem has the lab at a standstill but willing to allow us the freedom to pursue our own ideas.

I would like to express my most sincere gratitude to my mentor Joseph M Cardon for being patient with me throughout my multitude of questions. Without his guidance and persistent help this thesis would not have been possible. I am indebted to him for his extraordinary mentorship, and his hard work and dedication were inspiring to me during his doctoral work.

I also want to thank my committee members, Professor Matthew Law and Professor Reginald Penner, for serving on my thesis committee. I admire each of them for their outstanding knowledge inspiring me to follow their example of conducting research at the highest level.

A huge part of what made the Ardo lab a wonderful place to be a part of was my awesome labmates. I am grateful for all of them. It has been great working with all of you and I look forward to hearing about all of your successes in the future. I have to thank my friends who have made my life happier. Most of all, thanks to Haniyeh and Nikki for always being willing to chat for hours, to laugh uproariously at the absurdity of life, and for always getting me. You have been amazingly supportive and I am uncommonly lucky to have found friends like you.

I have been blessed in many ways, but one of the blessings that I make sure to count twice is my family. My family are the ones to whom I truly owe all my accomplishments. My maman Shahin and baba Mahmoud, and my sister Leyla have been my constant support system since before I can even remember, and without their compassion and their love, I would be nowhere. Though, geographically apart, they are always with me, and their love and support mean the world to me. They have given me all the riches that life could offer and without them, I would never be where I stand today. I will be forever thankful, and I know I can never make up for all their sacrifice. Maman, you mean more to me than words can even say, and no one will ever know the strength of my love for you. You have done almost everything imaginable you could do to make sure I was cared for and safe. I cherish

all your guidance, love, and prayers. Baba, thank you for giving me the confidence and courage to make the choices I have; from moving to U.S. and attending graduate school, to figuring out what I wanted to do and doing it. Your words of wisdom and encouragement have helped me through so much. Leyla, thank you for never giving up on me and always remaining by my side. Your inner strength inspires and pushes me to constantly do better. You have always been there whenever I needed someone to lean on through all of life's trials, and I will be eternally grateful for that. Most of all, thank you for making me a proud aunt to my adorable nephew, Darian. I would like to thank my brother-in-law Ardavan, who has really become a caring brother to me.

Lastly, I would like to thank my Hamidreza who has remained a constant pillar of support, comfort, and unending love. Without his love and encouragement, this work was not possible. He has been there for me throughout the absolute best and worst parts of graduate school, and his support helped me persevere even when I was not sure I could, largely by reminding me constantly of what I was capable of when I needed to hear it the most. Hamidreza, you have helped me remain stable in times of instability, and guided me in my moments of confusion. You are my role model, and I love you to no end.

ABSTRACT OF THE THESIS

Fabrication and Characterization of Dye-Sensitized Solar Cells with Efficient Regeneration Between Oxidized Dyes and Reduced Redox Shuttle Species

By

Nazila Farhang

Master of Science in Chemical and Biochemical Engineering

University of California, Irvine, 2019

Professor Shane Ardo, Chair

Dye-sensitized solar cells are a potential low-cost alternative to silicon solar cells. A current limitation to DSSCs is that most dyes used in these cells have bandgaps that are too large for ideal sunlight absorption. In this thesis, *cis*-Os(dcbpy)$_2$I$_2$ dye, a sensitizer with an absorption onset near 1.2 eV is introduced that has significantly better light-absorbing capability in the near-infrared spectral regions compared to benchmark RuN3, and related, dyes. To understand the effect of overpotential required to drive iodide/triiodide redox chemistry on the performance of DSSCs containing RuN3 or OsI$_2$ dyes bound to TiO$_2$, their performance was examined with varied ratios of $[I^-]$ to $[I_3^-]$. Measurements showed that the maximum light-to-electrical power conversion efficiency for RuN3 DSSCs occurred at an electrolyte potential of 0.35 V corresponded to 6.3 times more I^- than I_3^-. Whereas for OsI$_2$ DSSCs, an insignificant amount of power was generated due to slow electron-transfer kinetics between the redox shuttle and OsI$_2$. It was proposed that the addition of dmFc to the electrolyte could improve OsI$_2$ DSSCs performance by directly catalyzing I^- oxidation. To validate this hypothesis, foot-of-the-wave analysis was applied to the cyclic

voltammetry responses of TiO_2 photoelectrodes dyed with OsI_2. It demonstrated that dmFc catalyzed I_3^- reduction faster than I^- oxidation. Photoelectrochemical measurements unexpectedly showed that at the presence of dmFc in the electrolyte of OsI_2 DSSCs, electrons transferred from excited OsI_2 to the electrolyte solution, instead of injecting into the TiO_2 film, making these films photocathodic even though TiO_2 is n-type.

Chapter 1

Introduction

Solar energy has shown its advantages and potential among all the renewable energy sources for reliable power generation. The amount of solar radiation that earth receives each year is 3.8 million EJ, which is approximately 10,000 times more than current annul energy needs [1]. Therefore, in terms of energy conservation and environmental protection the direct conversion of solar radiation energy into electrical power through the use of photovoltaic devices is greatly desired.

1.1 Photovoltaic Energy Conversion

The principle of direct transformation of electromagnetic (i.e., light, including infrared, visible, and ultraviolet) energy into electrical energy in the form of current and voltage is known as photovoltaic energy conversion. Every photovoltaic energy conversion device requires four basic steps, some of which can occur simultaneously, which are [2], [3]

- A photon absorption process that excites electrons in the absorbing material bringing it from its ground-state to an electronic excited-state;
- A charge generation process that transforms the excited state into mobile negative and positive charge-carrier pairs;
- A charge separation process that results in separation of mobile negative charged carriers and mobile positive charged carriers in opposite directions;

- Charge recombination processes that ultimately result in loss of the photogenerated mobile negative and mobile positive charge carriers.

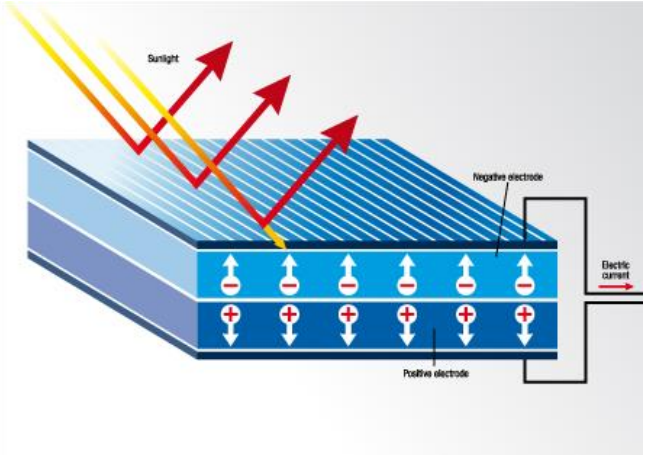

Figure 1.1: The cross-section of a typical solar cell

Devices that can efficiently convert energy in solar radiation into usable electrical energy are known as solar cells or solar photovoltaic devices. Photovoltaic devices can be designed to be effective for electromagnetic spectra other than sunlight. For example, devices can be designed to convert radiated heat (infrared light) into usable electrical energy.

Although photovoltaic technology is particularly attractive for the conversion of sunlight into electricity energy, up to now, commercially available photovoltaic technologies have been mostly limited to inorganic materials, which require expensive and highly energy consuming preparation methods. In addition, several of those materials, such as CdTe, are toxic and have low natural abundance. Alternatively, dye-sensitized solar cells (DSSCs) are well known as potential cost-effective photovoltaic devices because of inexpensive materials and simple fabrication process in comparison to inorganic, high-cost conventional crystalline silicon solar cells [3], [4].

1.2 Dye-Sensitized Solar Cells

DSSCs are potential low-cost solar cells belonging to the thin film solar cells group. Most DSSCs are composed of titanium dioxide (TiO_2) semiconductor, which is commonly used as a paint base in pigment industry, and a dye sensitizer that can be synthesized or extracted from a variety of natural resources with minimum costs [5], [6]. DSSCs are easy to fabricate, because of their relative insensitivity to environment contaminants and processability at ambient temperature [3].

In general, a DSSC commonly contains five components; a mechanical support that is coated with transparent conductive oxides (TCO), TiO_2 as the semiconductor film, a sensitizer that is adsorbed onto the semiconductor surface, an electrolyte that contains a redox mediator, and a counter electrode that regenerates the redox mediator. A schematic representation of a DSSC that shows the basic operating principle is shown in Figure 1.2.

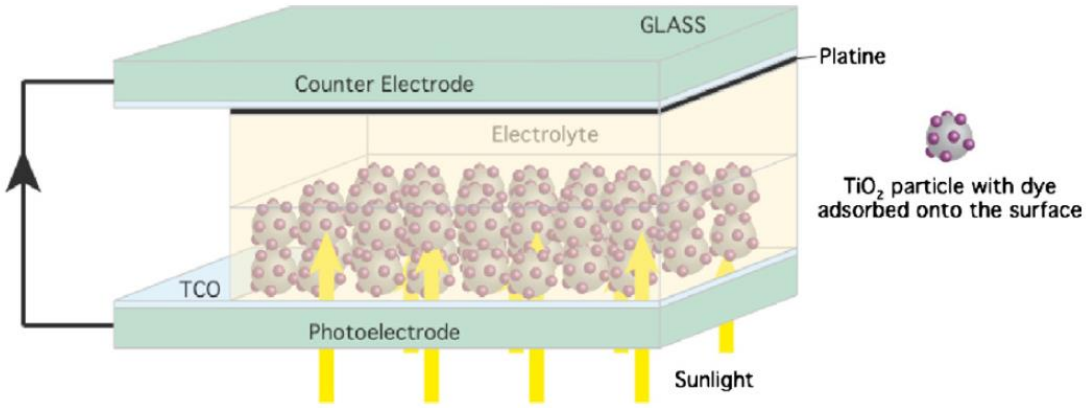

Figure 1.2: A schematic representation of the dye-sensitized solar cell [3].

In a DSSC each part of the device heavily influences the cost and efficiency of the cell. Therefore, the challenge of DSSC engineering is to fine-tune every component and

determine the ideal conditions to optimize the overall performance in the assembled device. Thus, in the past almost all research effort has been focused on the modification of each component for practical applications [7], [8]. A good amount of research has been done on improving the TiO_2-based photoelectrodes with emphasis on high specific surface area, large light scattering effect, enhanced interface quality, fast electron transfer, and enhanced charge collection capability [9]–[11].

The sensitizer or dye which adheres to the anode, has a significant role in capturing light energy. Hence, researchers have attempted to synthesize new dyes that would improve the cell efficiency such as preparation of four artificial chlorin-type sensitizers [12], D-A-π-A indoline dyes (XS45 and XS46) with different additional donors [13], and three organic dyes from C219 with different electron donors to further improve the open-circuit photovoltage of the cell [14].

Liquid electrolytes are another major component of DSSCs with some drawbacks such as poor long-term stability due to evaporation, leakage, flammability of organic liquids, and decomposition of the dye. To overcome these challenges, quasi-solid polymer electrolytes have been used but the conversion efficiencies obtained are relatively poor compared to those with liquid electrolytes [15]. In another study the mixture of an iodide salt system with two dissimilar cations made with polyvinylidene fluoride-based gel was used to increase the efficiency of cells [16].

1.3 Narrow Bandgap Sensitizers

There are various organic and organometallic dyes that are employed in DSSCs as a sensitizer for nanocrystalline anatase TiO_2. The breadth and intensity of the absorption of

light by the sensitizer contributes to the light-to-electrical power conversion efficiency of a DSSC [17]. Therefore, the properties of sensitizers, including the optical bandgap and ground-state reduction potential to oxidize the dye, affect the performance of DSSCs significantly [18]. According to the Shockley–Queisser limit for the maximum theoretical efficiency of a single junction solar cell, the maximum possible solar conversion efficiency is

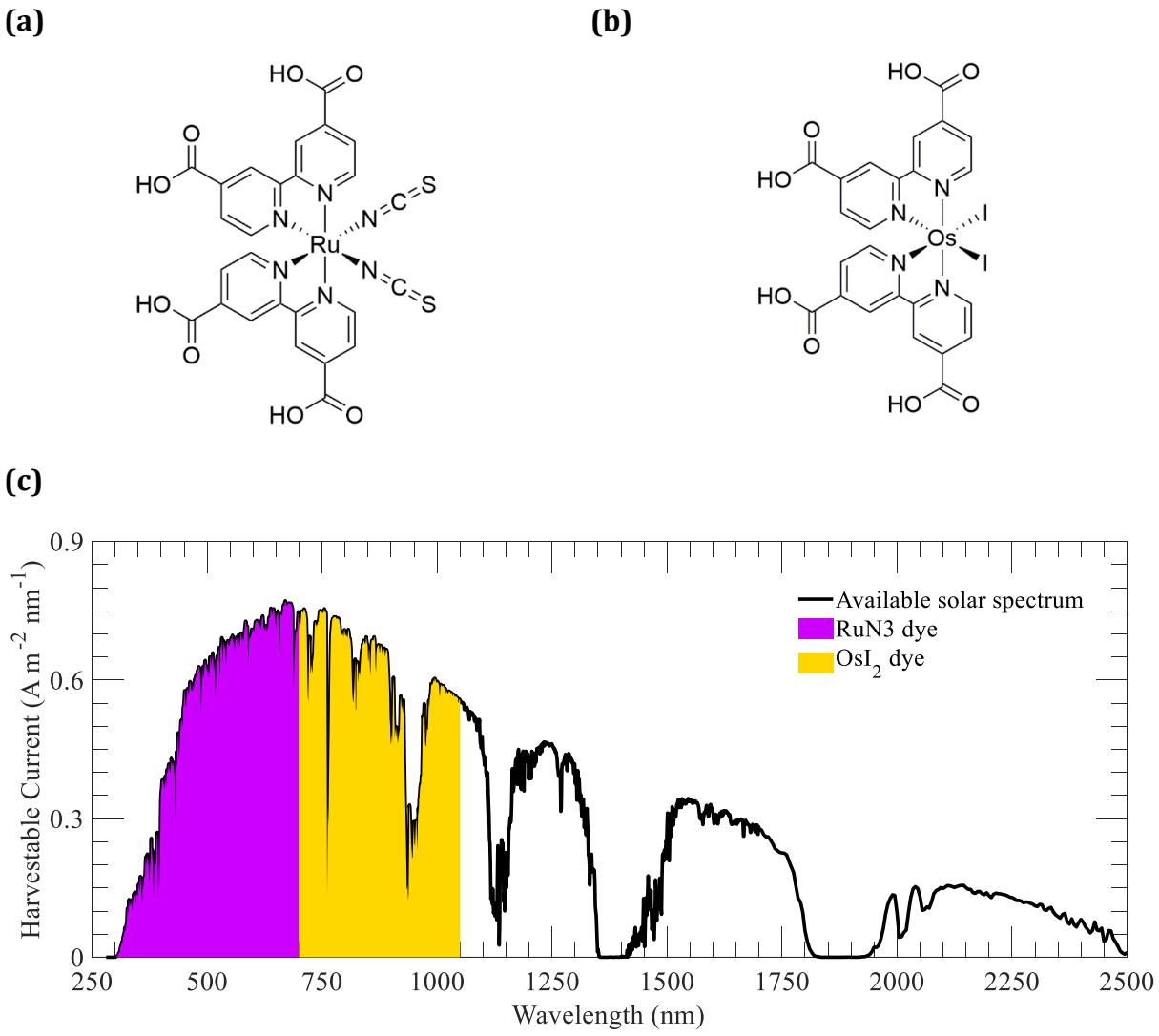

Figure 1.3: Molecular structure of (a) RuN3 dye and (b) OsI_2 dye. (c) Possible current available from the solar spectrum at 1 Sun of AM 1.5G sunlight, i.e., global 37° tilt. The area shaded in purple is the solar spectrum harvestable by RuN3 dye (250 – 700 nm), and the yellow area shows the additional light that can be harvested by OsI_2 dye (250 – 1050 nm).

30 – 34% and occurs at a bandgap of 1.1 – 1.4 eV under 1 sun of AM 1.5G sunlight. RuN3 dye is a state-of-the-art benchmark dye for DSSCs with more than 11% efficiency [19]. However, the optical bandgap of RuN3 dye – which is the difference in energy between its highest occupied molecular orbital and lowest unoccupied molecular orbital – is 1.8 eV, which corresponds to a 700 nm photon and is far from the ideal bandgap of 1.1 – 1.34 eV for best solar absorption. In other words, RuN3 dyes cannot absorb light with energy below its 1.8 eV bandgap, so red and infrared photons do not contribute to power production. Thus, it is desirable to use dyes with narrower bandgap. OsI_2 dye is an organometallic dye proposed in this thesis as a sensitizer that has an optical bandgap of 1050 nm, which is equivalent to 1.18 eV. The ground-state reduction potential to oxidize OsI_2 is +0.23 V vs SCE. The light-absorbing capability of OsI_2 dye in the red and near-infrared regions is better than RuN3 dye. Therefore, it is expected that DSSCs incorporating OsI_2 dye will generate more power than DSSCs fabricated with RuN3 dye under given operating conditions. Figure 1.3 illustrates RuN3 and OsI_2 dyes structure and the solar spectrum harvestable by these dyes.

1.4 Thesis Outline

The primary objective of Chapter 2 is to understand the effect of redox shuttle overpotential relative to dye ground-state potential on the performance of TiO_2 based DSSCs. For this purpose, the performance of DSSCs were examined under varied concentrations of I^- and I_3^-, the components of the redox shuttle in the electrolyte solution. Two groups of DSSCs were fabricated and tested in this chapter, the sensitizer in the first group was RuN3 dye and in the second group it was OsI_2 dye. Through

photoelectrochemical measurements critical parameters in characterization of a solar cell were determined for these DSSCs. Since OsI_2 dye has a narrower bandgap than RuN3 dye, it was expected that DSSCs fabricated with OsI_2 dye would have a higher light-to-electrical power conversion efficiency, however this was not observed to be the case.

Chapter 3 examines the role of dmFc as an electrocatalyst on electron-transfer rate at TiO_2-dye/electrolyte interfaces. First, it was shown that dye molecules bound to a mesoporous surface of anatase TiO_2 films have a non-ideal Nernstian redox behavior. Thus, a non-ideality factor was introduced to modify the Nernst equation which was measured by performing potential step chronoamperometry on the dyed mesoporous TiO_2 photoelectrodes. The effect of dmFc on the catalysis of I^- oxidation and I_3^- reduction was then studied by performing cyclic voltammetry measurements on single TiO_2 photoelectrodes dyed with OsI_2. To avoid experimental distortions that occur at high current densities, foot-of-the-wave analysis was applied to the cyclic voltammetry responses to extract kinetic information at low current densities where catalytic response is unperturbed. The modified Nernst equation was necessary to correctly perform foot-of-the-wave analysis.

Chapter 4 examines the hypothesis that the addition of dmFc to the electrolyte solution of OsI_2 DSSCs can improve the kinetics of charge-transfer between the redox shuttle and OsI_2 dye. OsI_2 DSSCs containing dmFc, a fast single-electron transfer reagent, were fabricated similar to Chapter 2 and the performance these DSSCs was examined by performing photoelectrochemical measurements.

Chapter 2

DSSCs without Additives

2.1 Introduction

Our goal in this chapter is to determine the optimal electrolyte potential for dye-sensitized solar cells containing $Ru(dcbpy)_2(NCS)_2$ (RuN3) or *cis*-$Os(dcbpy)_2I_2$ (OsI_2) dye sensitizers, which results in the maximum light-to-electrical power conversion efficiency. For this purpose, the performance of DSSCs are examined under varied concentrations of I^- and I_3^-, the components of the redox shuttle in the electrolyte solution. Afterward, the effects of electrolyte potential on the performance of DSSCs are studied.

The first step is to find reasonable ratios of $[I^-]$ to $[I_3^-]$ and the corresponding electrolyte potentials through calculations using the Nernst equation. Then electrolyte solutions are made using ratios of $[I^-]$ to $[I_3^-]$ based on the calculations, and those values are compared to experimentally measured potentials to investigate whether the actual electrolyte potential is the same as the calculated potential.

The next step is to fabricate and test different batches of DSSCs using titanium dioxide as the large bandgap, high-surface-area semiconductor support, the dye as the light absorber, and iodide/triiodide as the redox shuttle. Electrolyte solution is made in a similar manner as it is made for potential measurements. Two groups of DSSCs are fabricated in this chapter: those with RuN3, which is a benchmark dye commonly used in DSSCs studies, and those with OsI_2, a new dye developed for these studies. The absorption onset for OsI_2 is

1050 nm, or 1.18 eV, which is approximately the same as crystalline silicon. A solar simulator and a potentiostat are used to test the performance of RuN3 and OsI_2 DSSCs by performing photoelectrochemical measurements including open-circuit potential (OCP), cyclic voltammetry (CV) and potential-driven electrochemical impedance spectroscopy (EIS). Through these measurements short-circuit photocurrent density (J_{SC}), open-circuit photovoltage (V_{OC}) and light-to-electrical power conversion efficiency of DSSCs with varied ratios of redox shuttle components are determined. To study the fluence dependence of DSSCs, neutral density light filters with different optical densities are used to attenuate the incident light from ~1 sun intensity to ~1/16 sun intensity. Lastly, for OsI_2 DSSCs ultraviolet–visible spectroscopy is conducted to measure the stability of solar cells during the photoelectrochemical measurements.

2.2 Experimental

2.2.1 Preparation of DSSC Electrolyte Solutions

To make the electrolyte, LiI_3 and LiI were mixed together so that $[I^-]$ and $[I_3^-]$ in the electrolyte are the concentrations given in Table 2.3. Since the concentration of I_3^- in the first two rows of Table 2.3 is insignificant, these two rows were eliminated. Therefore, ten batches of DSSC solutions were made with different ratios of $[I^-]$ to $[I_3^-]$. For instance, to make the first batch of DSSCs with the electrolyte potential of 0.29 V, based on Table 2.3, 99.8% of the solution is made up of a stock solution of LiI and the remaining 0.2% using a stock solution of LiI_3. LiI_3 stock solution was composed of 0.46 M lithium iodide (99%, anhydrous, Acros Organics), 0.46 M iodine (99.8%, Spectrum Chemical Mfg. Corp.), 0.02 M

trifluoroacetic acid (Oakwood Chemicals), 0.07 M tetra-*n*-butylammonium perchlorate (98%, TCI), 85% vol acetonitrile (ACS/HPLC 99.9%, Fisher Chemical) and 15% vol valeronitrile (99.5% Aldrich). All the components and their quantities in LiI solution were the same as those of LiI_3 except that there is no addition of iodine.

2.2.2 Measurement of Solution Potential

Three-electrode photoelectrochemical measurements were performed to measure the potential of the electrolyte solution of the DSSCs. A platinum 5μm ultramicroelectrode (UME) working electrode, a platinum mesh counter electrode, and an aqueous KCl-saturated calomel reference electrode (SCE) were used. Before performing any measurements, the working electrode was polished with MicroPolish alumina powder (CH Instruments, Inc.) three times with particle sizes of 1.00 μ, 0.30 μ and 0.05 μ.

For each solution, 10 mL of electrolyte solution, the working electrode, the reference electrode, and the counter electrode were added to an electrochemical beaker. The electrodes were connected to a Bio-Logic VSP-300 potentiostat. A 1-min open-circuit potential measurement was followed by cyclic voltammetry with a starting potential of 0 V versus E_{OC}, a scan rate of 10 mVs^{-1}, and lower and upper scan limits of –0.5 V and +0.5 V versus reference.

2.2.3 Preparation of Dye-Sensitized Solar Cells

Synthesis and Preparation of TiO_2 Nanoparticle Paste

TiO_2 paste was prepared according to general protocol presented in the experimental section of Ref. [20]. This procedure is for the synthesis of a TiO_2 nanoparticle

suspension with particles of approximate average diameter of 20 nm and it is scaled down to 1/10th of the amounts presented in Ref. [20] so that all the TiO_2 solution can be transferred to the Teflon liner.

To synthesize a TiO_2 colloid suspension, 5.86 g titanium (IV) isopropoxide (≥98%, Acros Organics) was massed out into a 20 mL vial containing a stir bar and then was stirred on a stir/hot plate. 1.20 g glacial acetic (ACS 99.7%, EMD) was added to the vial by a syringe without a needle; this reaction is exothermic. The mixture stirred at a room temperature for 15 minutes and then was added to a 125 mL Erlenmeyer flask containing a 1.25" stir bar and 29 mL of deionized water. It was stirred on a stir/hot plate at 700 rpm in a room temperature water bath for 60 min. A translucent white slurry formed after 60 min that broke up over time. 0.4 mL concentrated nitric acid (ACS 68 – 70%, Macron Fine Chemicals) was added to the slurry and the bath temperature was raised first to 50 °C and then 80 °C. It was stirred for 75 min at 80 °C and most of the contents of slurry dissolved. The water bath was allowed to cool to a room temperature and the mixture was transferred to a Teflon liner. Deionized water was added until the total volume equaled 37 mL. The Teflon liner was placed in a steel pressure vessel and then heated at a rate of 8 °C min^{-1} to 220 °C and held for 12 h in a muffle furnace (Sentry Xpress 4.0, Paragon Kiln). When the temperature returned to a room temperature, the solution inside the Teflon liner was mixed for a few minutes using an ultrasonic horn. The supernatant was then removed by centrifuging and was replaced by ethanol (proof 200, Rossville Gold Shield USP). This step is repeated three times and on the third time, ethanol is added such that the final solution contains 40 wt% TiO_2 or weighed 4.1 g. Meanwhile, a 10 wt% solution of ethyl cellulose 5 – 15 mPa.s (6% in toluene/ethanol 80:20 (25 °C), 48.0 – 49.5%, w/w ethyloxyl

basis, Sigma) and ethyl cellulose 30-50 mPa.s (5% in toluene/ethanol 80:20 (25 °C), 48.0 – 49.5%, w/w ethyloxyl basis, Sigma) in ethanol was prepared and stirred for at least 12 h prior to use. 6.49 g of terpineol was mixed to 4.0 g of the 40 wt% TiO_2 solution and then 4.5 g of ethyl cellulose 5 – 15 mPa.s solution and 3.5 g of ethyl cellulose 30 – 50 mPa.s solution were added to the mixture. The mixture was diluted with 8 mL of ethanol and then transferred to a 40 mL vial. It was then sonicated in the ultrasonic bath and then sonicated by using the ultrasonic horn three times. The homogenized mixture was concentrated by rotary evaporator by removing 17.66 g ethanol and a thick TiO_2 paste is produced.

Preparation of Dye-Sensitized Solar Cells

Glass Cutting and Drilling

In DSSCs the electrolyte solution is sandwiched between two slides of electrically conductive glasses. One of the slides acts as a working electrode and is partially coated with TiO_2 paste and the other slide is a counter electrode and is covered with platinum nanoparticles.

First, two 2 cm × 3 cm fluorine-doped tin oxide (FTO) glass slides (TEC7, 2.2mm, GreatCell Solar Limited) were prepared and two holes were drilled in the counter electrode with a drill press (SKIL 3320-01 10") equipped with a 1 mm diamond grinding drill bit

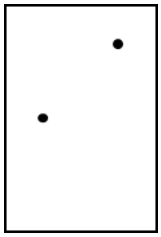

Figure 2.1: Counter electrode hole marking template

according to the counter electrode hole marking template.

Glass Cleaning

The glass slides were first sonicated in 5-10% wt aqueous Alconox solution (powdered precision cleaner, Alconox, Inc.) for 15 min, rinsed with water and ethanol (proof 200, Rossville Gold Shield USP), sonicated in ethanol for 15 min, and rinsed with ethanol. The slides were allowed to dry and then heated to 550 °C on a hot plate for 1 h. The glass slides were allowed to return to a room temperature and immediately used in the next step.

TiO_2 Paste Application

TiO_2 paste was applied on a specified area of conductive side of the working electrode slide (Figure 2.2) by the doctor-blade method by applying parallel strips of Scotch 3M magic tape to the slide, applying a drop of TiO_2 paste to one edge of the slide between the pieces of tape, and then spreading the paste into a uniform thin layer between the pieces of tape by scraping with a Teflon coated razor blade (PTFE coated, 3-facet, Personna GEM).

Counter Electrode Platinization

Meanwhile, three drops of chloroplatinic acid hydrate in methanol (≥99.9% trace metals basis, Aldrich) was added to the conductive side of the counter electrode. Each drop of chloroplatinic acid hydrate was dripped in the center of the two fill holes and allowed to dry before the next drop was added.

Electrode Sintering and Calcinating

Both working electrode and counter electrode, were placed in a muffle furnace. The furnace was heated at a rate of 180 °C/h to 90 °C and held for 1 h, then heated at the same rate to 500 °C and held for 1 h. After cooling to a room temperature, excess TiO_2 was scratched off according to the template (Figure 2.3) by using a Teflon-coated razor blade. The area of the surface coated with TiO_2 was approximately 0.64 cm^2.

Figure 2.2: Doctor-blade location template

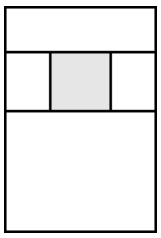

Figure 2.3: TiO_2 location template

$TiCl_4$ Application

The working electrode was coated with a uniform thin layer of TiO_2 by placing it in a covered glass petri dish and covering it with a 0.04 M titanium (IV) chloride solution (prepared from titanium (IV) chloride (99%, Strem Chemicals, Inc.)) and heating at 70 °C on a hot plate for 40 min and allowed to cool to room temperature. The working electrode is rinsed with water, allowed to dry at room temperature, and re-sintered with the same procedure described earlier.

Dyeing Procedure

For better adsorption of the dye on TiO_2, the working electrode slide was immersed in a petri dish filled with 1mM tetra-*n*-butylammonium hydroxide solution (diluted from

40% w/w aqueous solution, Alfa Aesar) for 15 min. It was rinsed by immersion in a petri dish filled with water for 15 min followed by immersion in a petri dish filled with acetonitrile (certified ACS 99.5%, Fisher Chemical) for 15 min. The working electrode slide was then placed in petri dish containing 2mM solution of dye in 1:1, v/v acetonitrile and methanol (certified ACS 99.9%, Fisher Chemical) which was then carefully sealed with parafilm (Parafilm® M) to prevent the evaporation of the solvent. The petri dish was covered with a aluminum foil overnight. The first group of DSSCs were fabricated with $Ru(dcbpy)_2(NCS)_2$ dye, abbreviated as RuN3, (85% (HPLC), Sigma Aldrich). The second group used *cis*-$Os(dcbpy)_2I_2$ dye, abbreviated as OsI_2, (synthesized by Joseph M Cardon, PhD candidate in Ardo Lab, UC Irvine).

Surlyn Gasket Preparation

While the working slides were in the dye bath, Surlyn (30 μm thermoplastic sealant, GreatCell Solar Limited) gaskets were prepared. These gaskets are cut out with a razor blade according to the gasket cutting template (Figure 2.4) and stored overnight in a desiccator.

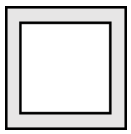

Figure 2.4: Gasket cutting template

Solar Cell Assembly

Immediately before assembly, dyed working electrodes were cleaned of weakly bound dyes by soaking for 15 min in 1:1, v/v acetonitrile and methanol solution, soaking

for 15 min in acetonitrile solution, and allowed to dry. A Surlyn gasket was placed on the platinum coated side of the counter electrode so that it surrounds both holes. The working electrode was placed on the counter electrode and Surlyn gasket so that the two conductive sides were facing each other and the TiO_2 was centered between the two holes and surrounded by the gasket. Each electrode had a lip overhanging the other electrode for purpose of electrical contact during testing. Figure 2.5 illustrates how the two electrodes and the Surlyn gasket are placed over each other.

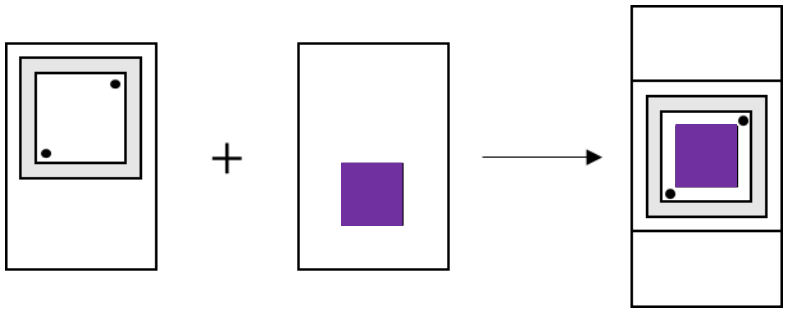

Figure 2.5: The placement of the electrodes and Surlyn gasket

The two slides and gasket were clamped together using two binder clips and placed in a preheated muffle furnace at 120 °C for 10 – 12 min to allow the Surlyn gasket to melt and seal the cell. The cell was allowed to cool to a room temperature before the binder clips were removed.

The solar cell was placed on the laboratory benchtop with the counter electrode holes facing up. A glass pipette was used to add a drop of redox electrolyte inside one of the holes so that it fills the cell. The redox electrolyte was made according to the procedure explained in subsection 2.2.1. Excess redox electrolyte was wiped off using a Kimwipe. To make an airtight seal, parafilm was rolled into two small compact rods and pressed into the

holes. Then surface of the counter electrode was painted with a thin layer of UV-cure nail polish (Lina UV Topcoat) and a 2 cm × 2 cm microscope glass slide (1.0 mm, VWR) was placed on top of the painted area. The microscope glass slide was gently wiggled to remove the bubbles beneath it and UV light from a UV flashlight was used to cure the nail polish. All the seams and junctions were painted with UV-cure nail polish and cured. Figure 2.6 shows samples of RuN3 and OsI_2 DSSCs, fabricated by going through the described procedure.

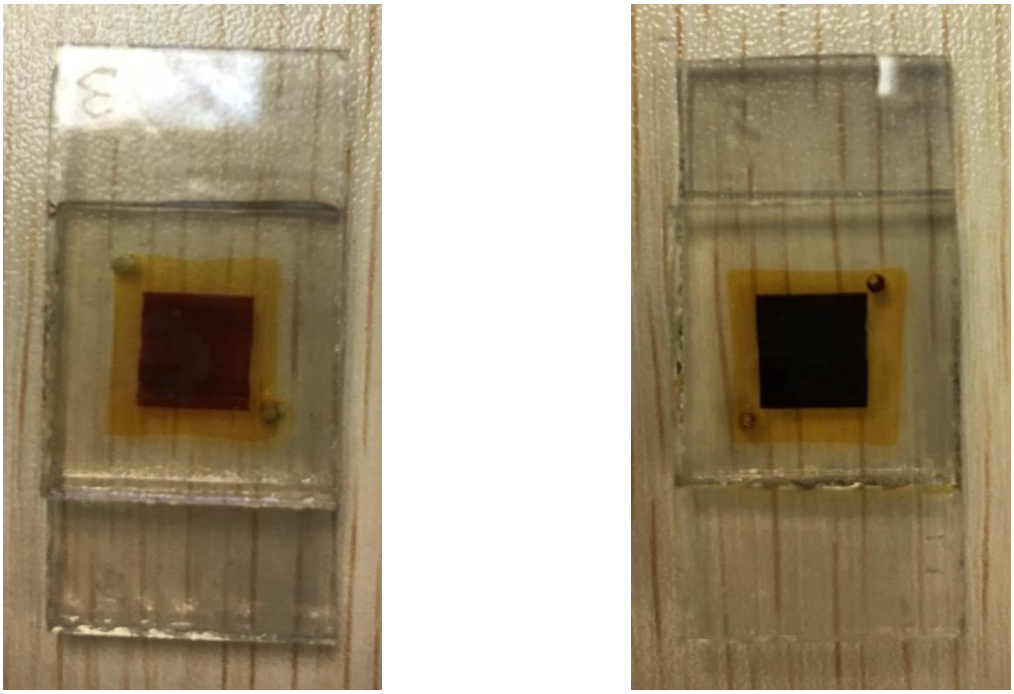

RuN3 DSSC OsI_2 DSSC

Figure 2.6: Fabricated samples of DSSCs by going through the procedure explained in subsection 2.2.3

2.2.4 Photoelectrochemical Characterization of Solar Cells

General procedures

Two-electrode photoelectrochemical measurements are carried out to test the performance of fabricated DSSCs. All two-electrode tests were performed by connecting the

dyed TiO_2 electrode to the working and the platinized FTO to the counter electrodes of a Bio-Logic VSP-300 potentiostat. A solar simulator (xenon arc lamp with air mass 1.5G filter, Oriel Instruments) was used as the light source. A calibrated silicon diode was connected to the potentiostat and placed in front of the solar simulator lamp. The diode's distance to the lamp was changed and its short-circuit current was measured by chronoamperometry until it became 4.72 mA which corresponds to 1 sun light intensity. This location was marked and the DSSCs were placed at this location for photoelectrochemical measurements.

Open-Circuit Voltage Measurement

A 30-second OCP test measured the DSSC potential without significant current passing through the sample. This test was performed primarily to ensure that the solar cell electrodes were connected to the potentiostat properly.

Cyclic Voltammetry Measurement

CV was used to measure the performance of solar cell with starting potential of 0 V versus E_{OC}, a scan rate of 100 mVs^{-1}, and upper and lower potential scan limits of 0.5 V and –1.0 V versus reference. Two cycles were performed and the results of the second were used in the final analysis.

Potentio-Electrochemical Impedance Spectroscopy Measurement

EIS was used to measure the resistance of the solar cell assembly. The potential was set to 0 V versus E_{OC}, with a frequency range between 1 kHz to 2 MHz collecting six points per decade and AC signal amplitude of 10 mV.

2.2.5 Fluence Dependence Measurement

A light fluence dependence measurement was performed to measure how light intensity affects the performance of DSSC. Neutral density (ND) filters (NEC01S-absorptive 2" × 2" ND filter kit, Thorlabs) were placed between the solar cell and solar simulator lamp which uniformly attenuated the light intensity of the solar simulator. In this measurement OD 0.3, OD 0.6, OD 0.9 and OD 1.2 filters were used which transmit 50.1%, 25.1%, 12.6% and 6.3% of light respectively. Additionally, a dark measurement was performed where the solar simulator lamp was covered. At each light fluence the OCP, CV, and EIS measurements were done as described above.

2.2.6 Solar Cell Area Measurement

Current density (J) gives information on the amount of the current that is passing through a unit area of the working electrode, in this case, the dyed TiO_2. To obtain the current density the area of TiO_2 thin film on the working electrode was measured. ImageJ, an image processing software, was used to measure the TiO_2 geometric surface area. This software expresses the results of length and area measurements in pixels and square pixels respectively. To convert pixel into cm, a ruler as a length measurement reference was placed next to a DSSC and the picture of reference ruler and DSSC was processed in ImageJ. First, 2 cm of the reference ruler was measured with the *straight selections* tool to check how many pixels formed a 2 cm length in that picture. Then the accurate area of the dyed TiO_2 was measured by the *polygon selections* tool in square pixels which can be converted into cm^2. Figure 2.7 is an example of a dyed area measurement of a RuN3 DSSC by ImageJ.

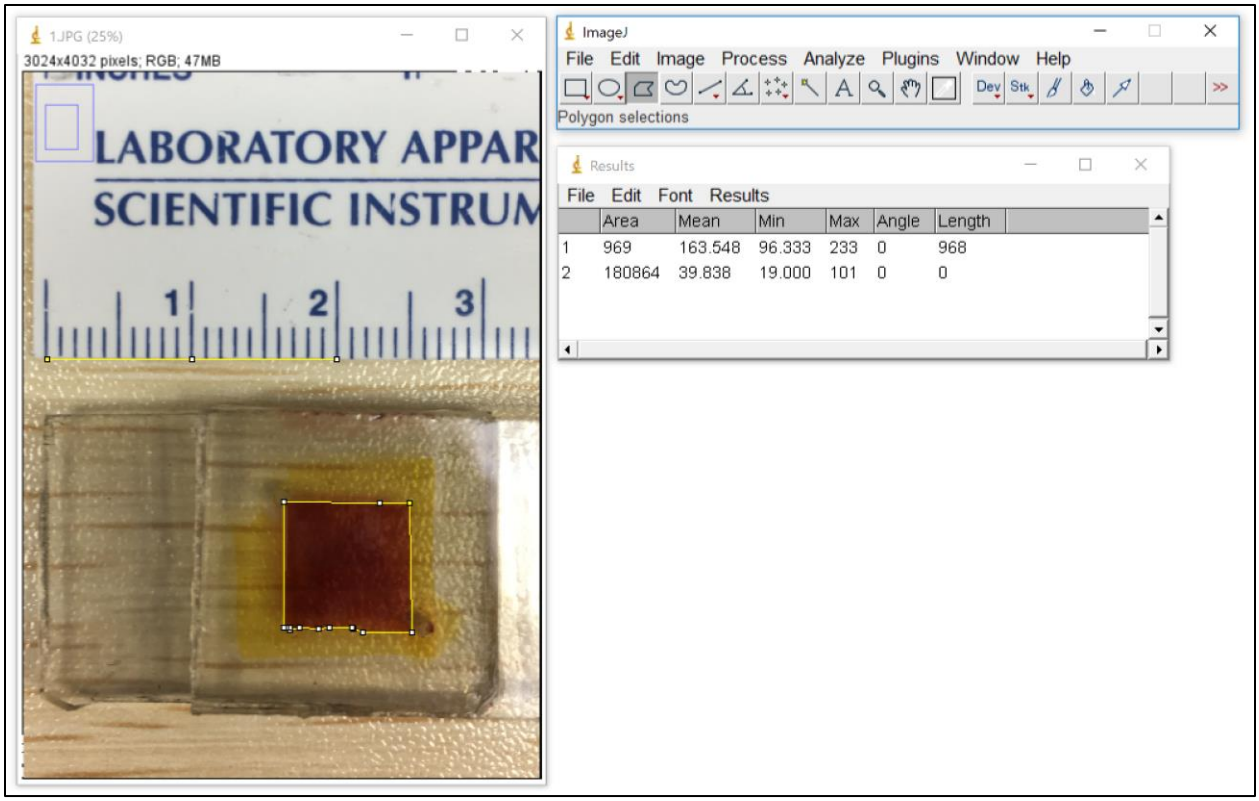

Figure 2.7: Illustration of dyed area measurement of a RuN3 DSSC by ImageJ

2.2.7 Ultraviolet–Visible Spectroscopy

Ultraviolet–visible spectroscopy (UV-Vis) was used to measure cell stability during the photoelectrochemical measurements. For this purpose, UV-Vis spectroscopy was carried out twice, once before photoelectrochemical testing and once after. The DSSC was placed in front of the sample holder of a UV-Vis spectrophotometer (Cary 60, Agilent Technologies) facing the incident beam. Before doing the spectroscopy, the baseline was set on *zero/baseline correction* and dark measurement was collected by blocking the sample beam and blank measurement was collected though air. The DSSC was aligned so the beam fully passed through the dyed area of the solar cell. An absorption spectrum of 1100 to 200 nm wavelengths with a scan rate of 600 nm min^{-1} was taken.

2.3 Results and Discussion

2.3.1 Calculating Redox Shuttle Potential

The redox shuttle which was used in these dye-sensitized solar cells was iodide/triiodide. The Nernst equation was used to calculate the redox shuttle potential,

$$E' = E'_0 - \frac{RT}{zF} ln \frac{[I^-]^3}{[I_3^-]} \quad (2.1)$$

Where

E': solution actual potential in V

E'_0: solution potential at standard conditions in V

R: the universal gas constant; R = 8.314472 J $K^{-1}mol^{-1}$

T: temperature in Kelvin

z: the number of electrons transferred in the cell reaction or half-reaction

F: the Faraday constant; $F = 9.648533 \times 10^4$ C mol^{-1}

$[I^-]$, $[I_3^-]$: iodide and triiodide concentrations respectively in M

Several standard potentials are reported for the iodide/triiodide system in acetonitrile but the general consensus is that standard redox potential of iodide/triiodide in acetonitrile is +0.354 to +0.29 V vs NHE (Normal Hydrogen Electrode) [21]. All the experiments which were carried out for the purpose of this thesis, were done at the temperature of 294.15 K (21 °C); therefore, for calculating E' with the Nernst equation, T is considered to be 294.15 K. The number of electrons transferred (z) in the reduction of I_3^- to I^- is 2.0

$$I_3^- + 2e^- \longrightarrow 3I^- \quad (2.2)$$

One of the most important steps in fabrication of DSSCs is to determine the ratio of $[I^-]$ to $[I_3^-]$ and to make the electrolyte solution based on this ratio. The first step to find the $[I^-]$ and $[I_3^-]$, is to determine the proper solution potential. Acetonitrile is the primary solvent of our DSSCs electrolyte and the saturation concentrations (C^{sat}) of I^- and I_3^- in acetonitrile are respectively 2 M and 0.46 M. Different values of E were calculated first by considering $[I^-]$ constant at C^{sat,I^-} and decreasing $[I_3^-]$ from C^{sat,I_3^-} by powers of 2 down to 0.001 M which is the lowest practical concentration that could be used in a DSSC, and second by doing the same procedure but $[I_3^-]$ was kept constant at C^{sat,I_3^-} and $[I^-]$ was decreased. Tables 2.1 and 2.2 show the calculated values of E based on these saturation concentrations and the Nernst equation.

Table 2.1: Calculated values of E' when $[I^-]$ is constant at C^{sat,I^-} in acetonitrile

	$[I^-]$ (M)	$[I_3^-]$ (M)	E (V)
1	2	0.46	0.314
2	2	0.23	0.305
3	2	0.115	0.296
4	2	0.0575	0.288
5	2	0.0287	0.279
6	2	0.0144	0.270
7	2	0.00719	0.261
8	2	0.00359	0.253
9	2	0.00180	0.244

Table 2.2: Calculated values of E' when $[I_3^-]$ is constant at C^{sat,I_3^-} in acetonitrile

	$[I^-]$ (M)	$[I_3^-]$ (M)	E (V)
1	2	0.46	0.314
2	1	0.46	0.3404
3	0.5	0.46	0.3664
4	0.25	0.46	0.393
5	0.125	0.46	0.419
6	0.0625	0.46	0.445
7	0.0312	0.46	0.471
8	0.0156	0.46	0.498
9	0.00781	0.46	0.524
10	0.00391	0.46	0.550
11	0.00195	0.46	0.576

From a purely mathematical standpoint the I^-/I_3^- redox couple should be able to produce any potential. However, from a realistic standpoint considering C^{sat,I^-} and C^{sat,I_3^-} in acetonitrile and a minimum reasonable concentration of 0.001 M, realistically achievable solution potentials range from about ~0.24 V to 0~.58 V.

Considering that the electrolyte solution consists of LiI and LiI_3 and that lithium ions are known to affect the conduction-band edge of TiO_2 it is important to have the same concentration of Li^+ in all solutions. It is also desirable to maximize the total quantity of redox shuttle in a solution to make the solar cells as conductive as possible and avoid resistive losses. Together, these two considerations yield Equation (2.3) which states that the sum of $[I^-]$ and $[I_3^-]$ should equal to the limiting saturation concentration, which is that of C^{sat,I_3^-} and equals 0.46 M.

$$[I_3^-] + [I^-] = 0.46 \text{ M} \tag{2.3}$$

At this stage, Equations (2.1) and (2.3) can be solved and used to calculate $[I^-]$ and $[I_3^-]$, which was accomplished by changing E' in the Nernst equation by steps of 0.03 V from 0.23 V to 0.56 V and calculating the two unknowns, $[I^-]$ and $[I_3^-]$.

Table 2.3: Values of $[I^-]$ and $[I_3^-]$ and the corresponding measured solution potential, E'

	$[I^-]$ (M)	$[I_3^-]$ (M)	E (V)
1	0.460	0.000007	0.23
2	0.460	0.000078	0.26
3	0.459	0.000837	0.29
4	0.451	0.00855	0.32
5	0.397	0.0627	0.35
6	0.263	0.197	0.38
7	0.140	0.320	0.41
8	0.0680	0.392	0.44
9	0.0317	0.428	0.47
10	0.0146	0.445	0.50
11	0.00664	0.453	0.53
12	0.00302	0.457	0.56

2.3.2 Comparison between Calculated and Measured Potentials of Electrolyte Solutions

The ratio of $[I^-]$ to $[I_3^-]$ in the electrolyte of RuN3 and OsI_2 DSSCs determines the electrolyte potential, which is a critical factor in DSSC performance. For both RuN3 and OsI_2 DSSCs, ten different batches of solar cells with different ratios of concentrations for the redox shuttle components in electrolyte were made. The composition of the ten redox shuttles was based on $[I^-]$ and $[I_3^-]$ cited in rows 3 to 12 of Table 2.3. According to the Nernst equation these compositions should result in the solution potentials presented in

for each corresponding row in the same table. The actual potential of the solutions was measured using cyclic voltammetry to ensure the same results are produced experimentally. It should be noted that the value of E_0' used in the calculation of potentials with the Nernst equation in Table 2.3, was measured versus normal hydrogen electrode in Ref. [21]. While in the measurement of the actual potentials, a saturated calomel electrode was used as the reference electrode and thus it is noteworthy that E' (SCE) = +0.241 V versus NHE at 20 °C. The results of the actual potential measurement of ten electrolyte solutions are given in Figure 2.8.

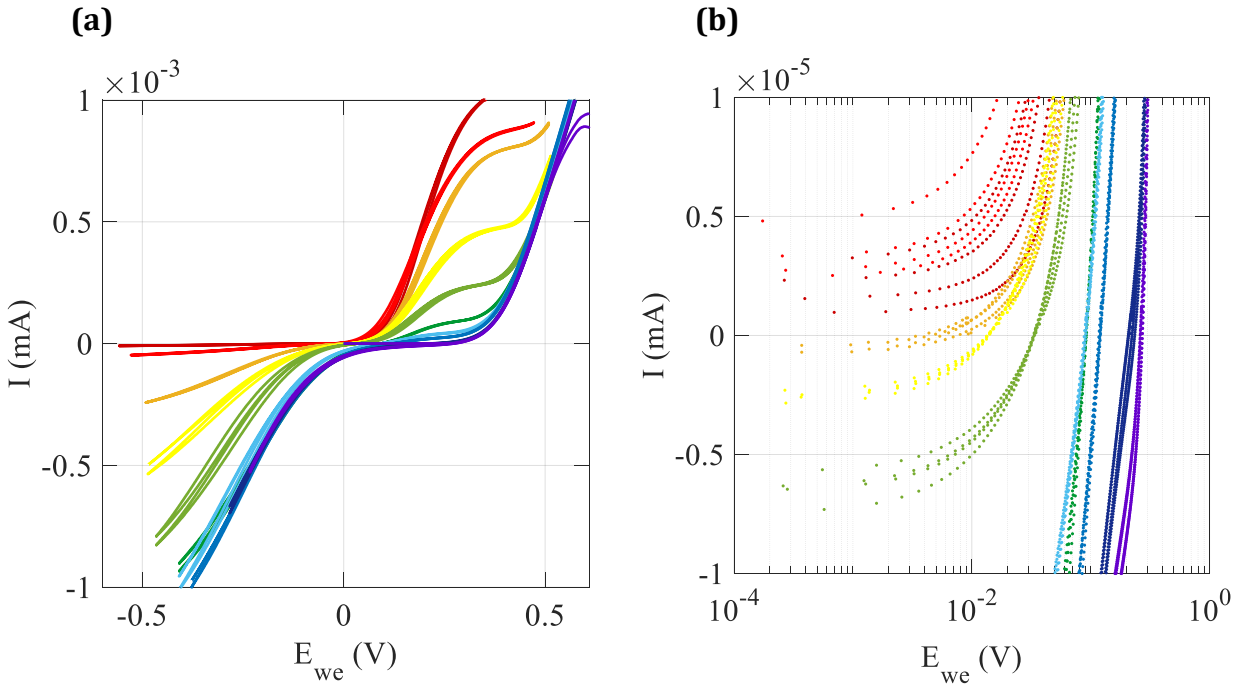

Figure 2.8: Cyclic voltammograms of ten electrolyte solutions is illustrated in (a) with both axes in linear scale and (b) with x-axis in logarithmic scale so it is clear where CV curves cross the x-axis. The ratio of $[I^-]$ to $[I_3^-]$ is decreased from 548.6 (red CV) to 0.007 (purple CV).

The platinum working electrode used for the photoelectrochemical measurements in Chapter 2, is an ultramicroelectrode. Ultramicroelectrodes are small with large edge-to-

volume ratios and therefore, the corresponding diffusional processes have a large contribution from radial diffusion even at early times. At slow enough scan rates all diffusion is radial and therefore constant with time allowing them to produce sigmoidal, non-hysteretic voltammograms (Figure 2.8 (a)) while electrodes of conventional size exhibit mass transport diffusion processes that are linear – not radial – meaning that the currents are time-dependent even at a fixed potential, which produces more commonly known hysteretic, "duck-shaped" voltammograms [22].

The iodide/triiodide redox reactions are asymmetric in that one is more reversible than the other. Triiodide reduction occurs by a rather simple mechanism involving only electron transfer. However, iodide oxidation occurs by a more complex mechanism that is an EC reaction, meaning an electron transfer (E) immediately followed by a chemical reaction (C). Therefore, the slope of the CV curves in Figure 2.8 (a) are different than those of symmetrical electrochemical systems.

The electron transfer and chemical reaction (i.e., EC mechanism) in the anodic polarization bias direction respectively read as

$$2I^- \longrightarrow I_2 + 2e^- \tag{2.4}$$

$$I_2 + I^- \longrightarrow I_3^- \tag{2.5}$$

The electron transfer in the cathodic polarization bias direction reads as

$$I_3^- + 2e^- \longrightarrow 3I^- \tag{2.6}$$

Electrochemical cells at equilibrium do not pass any net current. According to Gibbs free energy change equation for an electrochemical cell, the system reaches an equilibrium

when the potential of the working electrode (versus a reference electrode) is equal to electrolyte solution potential (versus the same reference electrode).

$$\Delta G = -nFE_{cell} \tag{2.7}$$

Therefore, to obtain the actual potential of the electrolyte solutions with different ratios of $[I^-]$ to $[I_3^-]$, the potential of the points at which the current is zero in Figure 2.8 are important, or in other words the x-intercepts. Table 2.4 compares the actual solution potentials obtained through CV measurements with calculated potential quantities from Table 2.3.

Table 2.4: Comparison between the calculated and measured quantities of the electrolyte potential

	$[I^-]$ (M)	$[I_3^-]$ (M)	ratio of $[I^-]$ to $[I_3^-]$	measured potential (V)	calculated potential (V)
1	0.459	0.000837	548.582	–0.0521	0.29
2	0.451	0.00855	52.770	–0.0286	0.32
3	0.397	0.0627	6.335	0.0054	0.35
4	0.2632	0.197	1.340	0.0138	0.38
5	0.140	0.320	0.439	0.0333	0.41
6	0.0680	0.392	0.174	0.0915	0.44
7	0.0317	0.428	0.074	0.0897	0.47
8	0.0146	0.445	0.033	0.119	0.50
9	0.00664	0.453	0.015	0.218	0.53
10	0.00302	0.457	0.007	0.266	0.56

The significant difference between the calculated and measured potentials could be due to several reasons. As explained before, one obvious reason is that different reference electrodes were used in the procedures of calculation and measurement of the potential of iodide/triiodide in acetonitrile solution. Another possible argument is that the conditions

in which E_0' was measured and used in calculations was different than those of measurement. For the purpose of potential calculations with the Nernst equation, it was assumed the electrolyte solution consisted of I^-, I_3^- and acetonitrile and the ambient temperature was 25 °C. However, for photoelectrochemical measurements, the prepared electrolyte solutions included I^- and I_3^- as redox shuttle components, acetonitrile and valeronitrile as solvents, and trifluoroacetic acid (TFA) and tetra-*n*-butylammonium perchlorate (tBP) as buffer components and the laboratory temperature was 21 °C. Moreover, the activity coefficients for I^- and I_3^- may differ from those used in prior measurements which would result in a shift in the potentials. Among all these disparities, the presence of TFA and tBP and thus, H^+ ions in the solution, most likely affects the measured potential the most, especially because the platinum working electrode is sensitive to H^+.

Another difficulty in this measurement is that, due to the asymmetry of the reaction mechanism for oxidation and reduction, the slope of each cyclic voltammogram near its open-circuit potential is very small. This means that even a small change in current due to oxidation or reduction of other species will cause a large change in measured open-circuit potential and that mass transport limitations for the slow reaction affect the value of the measured potential.

2.3.3 Characterization of RuN3 DSSCs

After the measurement of the potential of ten electrolyte solutions, ten batches of DSSCs were fabricated and tested to study the effect of electrolyte potential on the performance of DSSCs. The tests included OCP, CV, and EIS. The OCP measurement was

performed to make sure that each solar cell was connected to the potentiostat properly, the CV measurement gave information on the amount of the current that the DSSC passed at potentials between 0.5 to –1.0 V and the EIS measurement was performed in the frequency range of 1 kHz to 2 MHz where the impedance of the cell could be measured to learn about limiting factors in the potential–current relationship. Most notably, the impedance spectroscopy measurement was done to find where the impedance is fully real (*Re(Z)*). Figure 2.9 shows a Nyquist plot of the real part versus the imaginary part of the impedance where the frequency is varied. It can be seen from this figure that the impedance curve crosses the real axis at *Re(Z)* ≈ 27.5 Ω, which allows us to calculate corrected potentials as $E_c = E - Re(Z)I$.

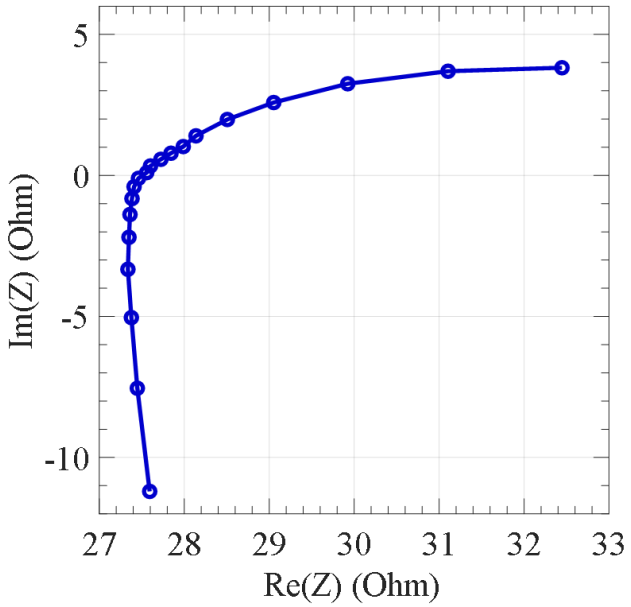

Figure 2.9: EIS plot of a RuN3 DSSC. The impedance of the solar cell becomes fully real at ~27.5 Ω where the imaginary impedance is zero.

J_{SC}, V_{OC}, and light-to-electrical power conversion efficiency are critical parameters in characterizing a solar cell. J_{SC} is the maximum current density that can be drawn from a

solar cell and it occurs when the load on the solar cell is zero, which occurs when the corrected potential equals zero. To remove the dependence on the surface area of the working electrode, this parameter is obtained by dividing the measured current by the area of solar cell as measured by using ImageJ software. V_{OC} is the maximum potential that a solar cell can generate to perform useful work in an external circuit and is measured when the current in the external circuit equals zero. The light-to-electrical power conversion efficiency is defined as the power generated per square centimeter of the solar cell divided by the power of incident light per square centimeter, also termed the irradiance.

The first group of the DSSCs contained the RuN3 dye, which is a state-of-the-art benchmark dye that is known to result in a large light-to-electrical power conversion efficiency. The results from experiments with RuN3-containing DSSCs are used as a positive

Table 2.5: The dependence of J_{SC}, V_{OC}, and efficiency values on the potential of the electrolyte solution of fabricated RuN3 DSSCs under 1 sun illumination intensity.

	ratio of $[I^-]$ to $[I_3^-]$	measured electrolyte potential (V)	calculated electrolyte potential (V)	actual J_{SC} (mA cm^{-2})	corrected J_{SC} (mA cm^{-2})	V_{OC} (V)	actual efficiency (%)	corrected efficiency (%)
1	548.582	–0.0521	0.29	10.36	11.94	–0.45	1.38	2.25
2	52.770	–0.0286	0.32	10.18	11.25	–0.43	1.42	2.42
3	6.335	0.0054	0.35	17.99	18.17	–0.58	3.33	6.40
4	1.340	0.0138	0.38	13.66	13.73	–0.51	2.59	4.78
5	0.439	0.0333	0.41	12.05	12.29	–0.54	2.42	4.60
6	0.174	0.0915	0.44	7.76	7.81	–0.52	1.76	2.77
7	0.074	0.0897	0.47	6.75	6.88	–0.44	1.03	1.59
8	0.033	0.119	0.50	1.93	1.96	–0.49	0.48	0.50
9	0.015	0.218	0.53	2.07	2.08	–0.58	0.72	0.77
10	0.007	0.266	0.56	2.32	2.34	–0.60	0.83	0.89

control measurement for experiments with OsI_2-containing DSSCs. The ground-state reduction potential to oxidize RuN3 is between +0.68 to +0.80 V vs SCE and its optical bandgap is 700 nm, which is equivalent to 1.8 eV. Table 2.5 shows the values of J_{SC}, V_{OC}, and efficiency for each batch of RuN3 DSSCs under 1 sun illumination intensity and obtained through the analysis of photoelectrochemical data. Corrected J_{SC} and corrected efficiency values are calculated with E_c. To ensure the results of the photoelectrochemical measurements are reproducible, for each batch three DSSCs were fabricated and the results of the measurements on three solar cells were averaged and reported.

As an example, shown in Figure 2.10 are the actual and resistance-corrected cyclic voltammograms of a third batch RuN3 solar cells with corresponding J_{SC}, V_{OC}, and maximum power point (P_{max}) values indicated.

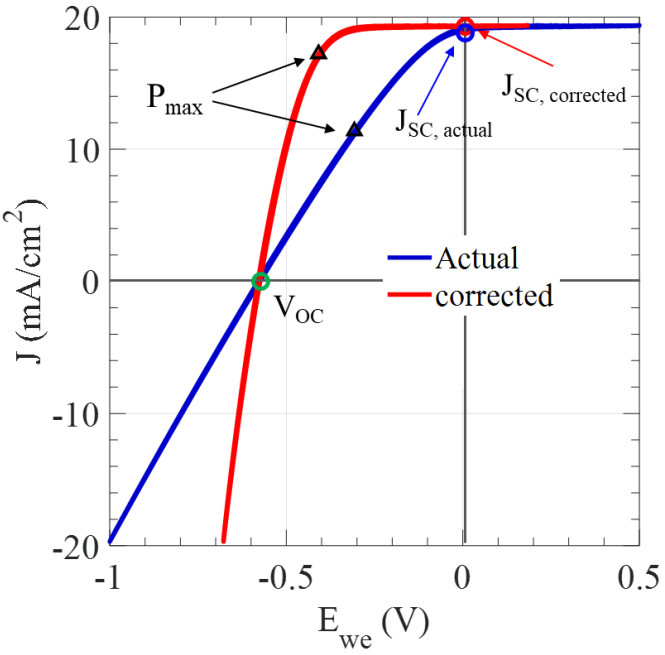

Figure 2.10: Cyclic voltammograms of a 3rd batch RuN3 DSSC at 1 sun illumination intensity. Measured and corrected CV curves are shown as well as their corresponding J_{SC}, V_{OC}, and P_{max} values.

Figures 2.11, 2.12, and 2.13 illustrate the changes in the values of J_{SC}, V_{OC}, and efficiency with the calculated potential of electrolyte solution under 1 sun illumination intensity in separate plots to clarify the dependency of these values to the electrolyte

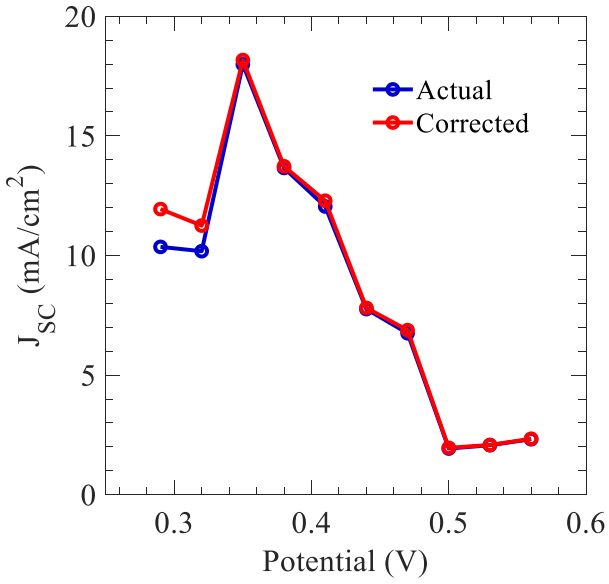

Figure 2.11: Changes in the values of actual and corrected J_{SC} with the calculated potential of electrolyte solution in RuN3 DSSCs under 1 sun illumination intensity.

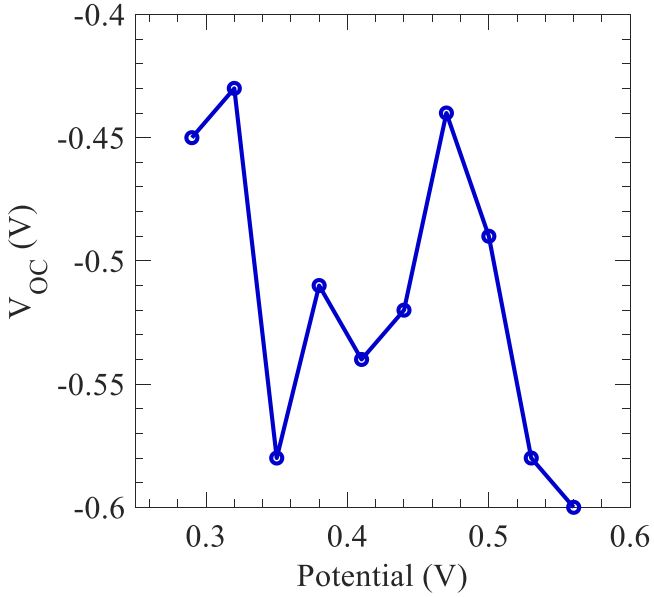

Figure 2.12: Changes in the values of V_{OC} with the calculated potential of electrolyte solution in RuN3 DSSCs under 1 sun illumination intensity.

potential. According to the Figure 2.12 there is no trend in the changes of open-circuit photovoltage with the electrolyte potential for the fabricated RuN3 DSSCs.

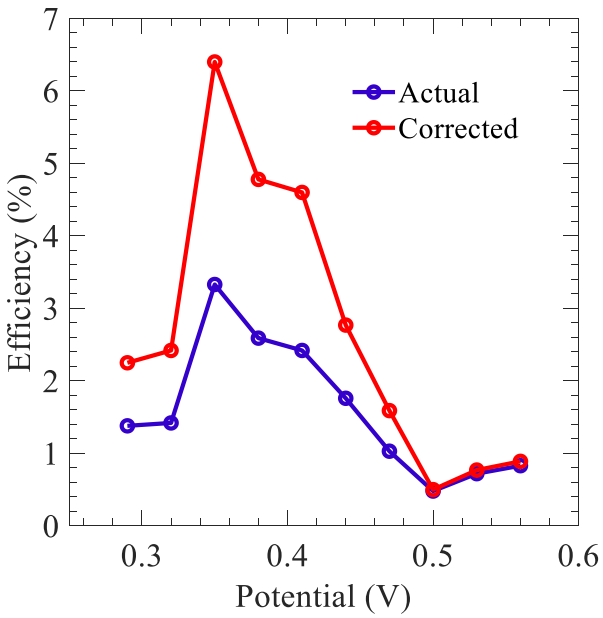

Figure 2.13: Changes in the values of actual and corrected efficiency with the calculated potential of electrolyte solution in RuN3 DSSCs under 1 sun illumination intensity.

Experimental observations show that the highest efficiency of fabricated RuN3 DSSCs happens when the calculated solution potential is 0.35 V. The difference between the actual and corrected highest efficiency is significant with values of 3.33% and 6.40% respectively.

To sum up, considering the values of J_{SC} and efficiency, under 1 sun illumination intensity the maximum power output occurs at the optimal electrolyte potential of 0.35 V (calculated) or 0.0054 V (measured) where the ratio of $[I^-]$ to $[I_3^-]$ is 6.335. The maximum power output occurs when there is enough I^- to quickly regenerate the dye, and there is enough I_3^- to quickly shuttle charge to the counter electrode. As long as these two conditions are satisfied, the RuN3 DSSC gives the best power output. In RuN3 DSSCs the

potential of Ru is positive enough that there is always significant driving force to perform rapid I^- oxidation. Experimentally this seems occurs at a $[I^-]$-to-$[I_3^-]$ ratio of 6.335.

In all the photoelectrochemical measurements neutral density light filters were used to vary the incident light intensity from 1 sun to 1/16 sun intensity. These fluence dependence measurements help to understand the effect of the intensity of the incident light on the performance of RuN3 and OsI_2 DSSCs. For this purpose, five ND filters with optical densities of OD 0.3, OD 0.6, OD 0.9 and OD 1.2 were used, that respectively transmit 50.1%, 25.1%, 12.6% and 6.3% of the incident light. Additional to using five ND filters, a dark measurement was performed where the solar simulator lamp was covered to study how much power a RuN3 DSSC can generate without intentional illumination. The fluence dependence measurements for RuN3 DSSCs show that regardless of the ratio of $[I^-]$ to $[I_3^-]$, by increasing the light intensity from 0 sun to 1 sun intensity, J_{SC} quantities increases roughly linearly, while the magnitude of V_{OC} increases nonlinearly. In all ten batches of

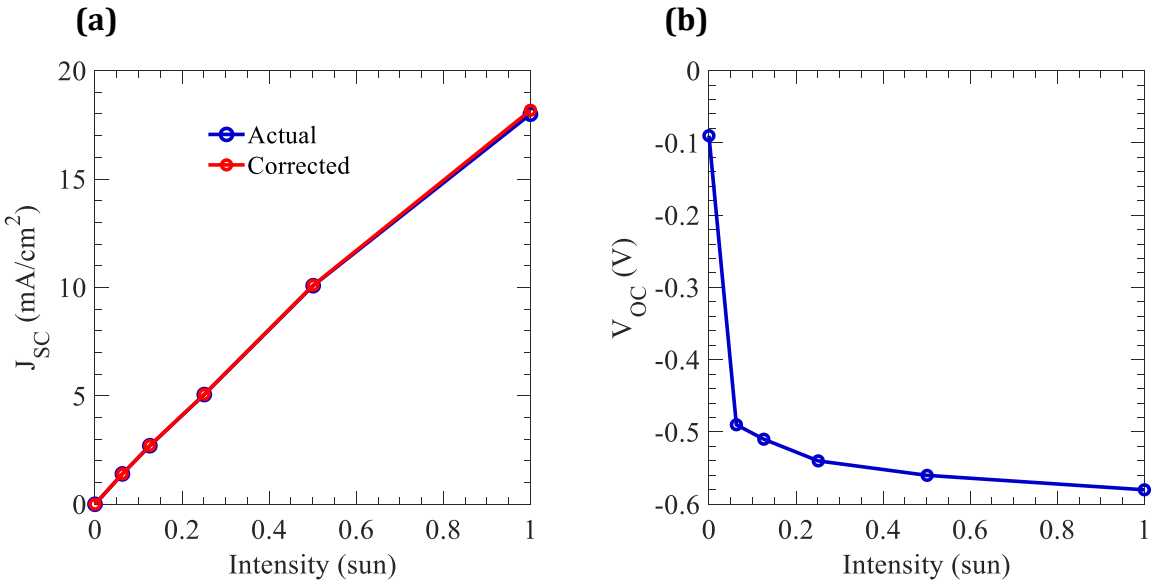

Figure 2.14: Fluence dependence of (a) actual and corrected J_{SC} and (b) V_{OC} values in the third batch of RuN3 DSSCs where the calculated electrolyte solution potential is 0.35 V.

RuN3 DSSCs the maximum efficiency occurred at 0.063 sun intensity.

The changes in quantities of J_{SC}, V_{OC}, and efficiency with respect to light intensity have the same trends for all the batches of RuN3 DSSCs. For instance, the results of fluence dependence measurement for the third batch, where the ratio of $[I^-]$ to $[I_3^-]$ is 6.335, are shown in Figure 2.14 and Table 2.6. Actual and corrected J_{SC} values have almost the same quantities at different light intensities.

Table 2.6: Fluence dependence of J_{SC}, V_{OC}, and efficiency values for the third batch of RuN3 DSSCs where the potential of electrolyte solution is 0.35 V (calculated) and $[I^-]$-to-$[I_3^-]$ ratio is 6.335.

fluence	incident light intensity (sun)	actual J_{SC} (mA cm^{-2})	corrected J_{SC} (mA cm^{-2})	V_{OC} (V)	actual efficiency (%)	corrected efficiency (%)
no filter	1	18.04	18.18	–0.55	3.18	5.76
OD 0.3	0.501	10.62	10.63	–0.53	4.83	6.97
OD 0.6	0.251	5.41	5.42	–0.51	6.07	7.31
OD 0.9	0.126	2.91	2.91	–0.48	7.09	7.85
OD 1.2	0.063	1.50	1.50	–0.46	7.67	8.09
dark	0	4.29E-03	4.29E-03	–0.13	0.0174	0.0175

2.3.4 Characterization of OsI_2 DSSCs

The second group of DSSCs incorporated the OsI_2 dye. These solar cells were fabricated and tested in the same manner as DSSCs made with RuN3 dye. The ground state reduction potential for oxidation of OsI_2 dye is +0.23 V vs SCE, which compared to RuN3 dye it is closer to the reduction potential of iodide/triiodide in acetonitrile. The optical bandgap of OsI_2 dye is 1050 nm, or 1.18 eV, which is approximately the same as the bandgap of crystalline silicon. OsI_2 dye absorbs more infrared light than RuN3 and

therefore is expected that DSSCs made with this dye would generate more power than RuN3 DSSCs; however, the photoelectrochemical measurements results do not initially support this hypothesis. Table 2.7 and Figures 2.15, 2.16, and 2.17 present the range of J_{SC}, V_{OC}, and efficiency values for each batch of OsI_2 DSSCs obtained through the analysis of photoelectrochemical data obtained using 1 sun illumination intensity.

Table 2.7: The dependence of J_{SC}, V_{OC}, and efficiency values on the potential of electrolyte solution of fabricated OsI_2 DSSCs under 1 sun illumination intensity.

	ratio of $[I^-]$ to $[I_3^-]$	measured electrolyte potential (V)	calculated electrolyte potential (V)	actual J_{SC} (mA cm^{-2})	corrected J_{SC} (mA cm^{-2})	V_{OC} (V)	actual efficiency (%)	corrected efficiency (%)
1	548.582	–0.0521	0.29	0.19	0.20	–0.162	0.0132	0.0133
2	52.770	–0.0286	0.32	0.09	0.10	–0.059	0.0021	0.0022
3	6.335	0.0054	0.35	0.08	0.12	–0.005	0.0013	0.0019
4	1.340	0.0138	0.38	0.08	0.11	–0.007	0.0002	0.0003
5	0.439	0.0333	0.41	0.04	0.06	–0.002	0.0002	0.0002
6	0.174	0.0915	0.44	0.06	0.10	–0.003	0.0004	0.0007
7	0.074	0.0897	0.47	0.09	0.13	–0.005	0.0014	0.0020
8	0.033	0.119	0.50	0.11	0.15	–0.007	0.0012	0.0016
9	0.015	0.218	0.53	0.13	0.21	–0.005	0.0005	0.0008
10	0.007	0.266	0.56	0.12	0.19	–0.005	0.0005	0.0007

According to Figure 2.15, there is no trend for the variations of actual and corrected J_{SC} quantities with the electrolyte potential. Except for the first two batches, the quantities of actual and corrected J_{SC} are fairly different. They also vary in different patterns; by increasing the electrolyte potential from 0.32 to 0.38 V (calculated quantities of potential)

the actual J_{SC} decreases from 0.32 to 0.35 V and then slightly increases from 0.35 to 0.38 V while the corrected J_{SC} first increases and then decreases at this potential range.

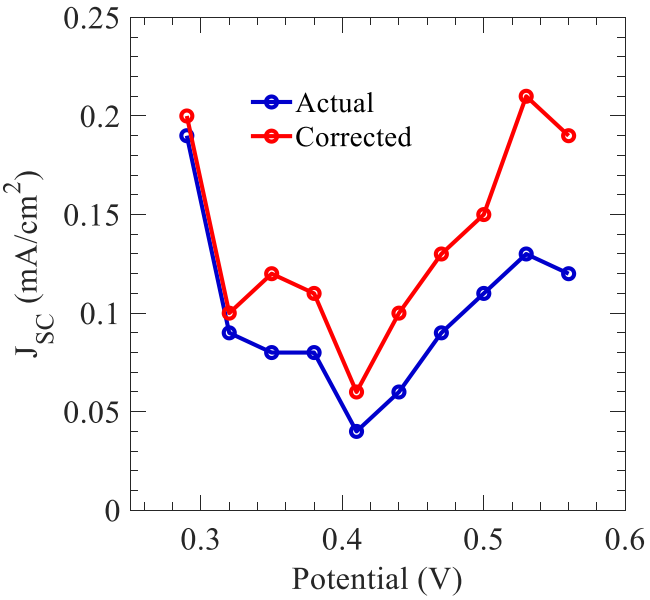

Figure 2.15: Changes in the values of actual and corrected J_{SC} with the calculated potential of electrolyte solution in OsI_2 DSSCs under 1 sun illumination intensity.

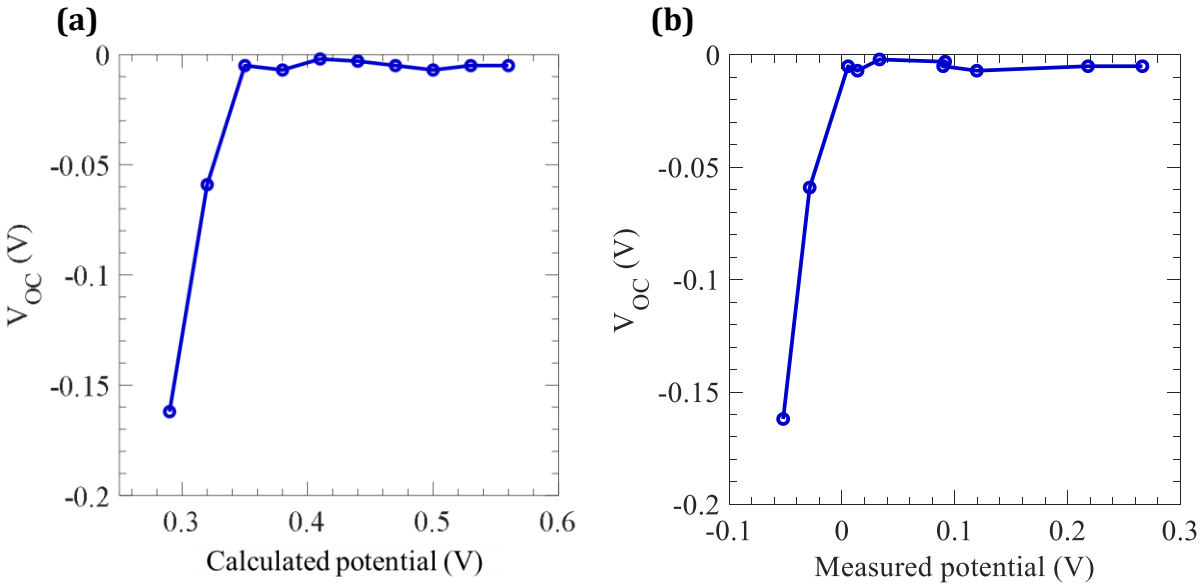

Figure 2.16: Changes in values of V_{OC} with the (a) calculated and (b) measured potentials of electrolyte solution in OsI_2 DSSCs under 1 sun illumination intensity.

As for V_{OC} variations with the electrolyte potential, for the first two batches it increases from –0.162 to –0.059 V and for the rest of the OsI_2 DSSCs by increasing the electrolyte potential, V_{OC} values are consistently close to –0.005 V.

Though it is expected that a solar cell using OsI_2 dyes is more efficient than a solar cell using RuN3 dyes, in all the batches of solar cells regardless of the electrolyte solution potential, the amount of power generated by OsI_2 DSSCs was insignificant. The maximum corrected efficiency of 0.0133% occurred using to the first batch of solar cells where the ratio of $[I^-]$ to $[I_3^-]$ is 548.582. This poor performance of OsI_2 DSSCs is probably due to very slow charge-transfer kinetics between the dye and redox shuttle or in other words, slow electron-transfer from the redox shuttle to the oxidized OsI_2 dye and will be discussed in more detail later in this thesis.

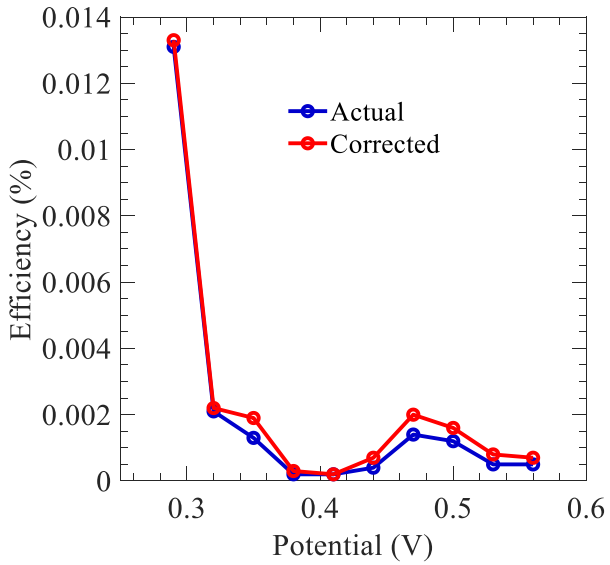

Figure 2.17: Changes in values of actual and corrected efficiency with the calculated potential of electrolyte solution in OsI_2 DSSCs under 1 sun illumination intensity.

The results of OsI_2 DSSCs fluence dependence measurements are similar to those of RuN3 DSSCs. For all the ten batches of solar cells with different electrolyte potentials, J_{SC}

and efficiency increase with the increase of the intensity of incident light from 0 sun to 1 sun intensity, while the V_{OC} values decrease. As an example, Table 2.8 and Figure 2.18 show the fluence dependence measurement results for the first batch of OsI_2 solar cells where the calculated and measured solution potentials are respectively 0.29 V and –0.0521 V.

Table 2.8: Fluence dependence of J_{SC}, V_{OC} and efficiency values for the first batch of OsI_2 DSSCs where the potential of electrolyte solution is 0.29 V (calculated) and $[I^-]$-to-$[I_3^-]$ ratio is 548.582.

fluence	incident light intensity (sun)	actual J_{SC} (mA cm^{-2})	corrected J_{SC} (mA cm^{-2})	V_{OC} (V)	actual efficiency (%)	corrected efficiency (%)
no filter	1	0.19	0.20	–0.16	0.013	0.013
OD 0.3	0.501	0.11	0.11	–0.13	0.011	0.011
OD 0.6	0.251	0.06	0.06	–0.08	0.007	0.007
OD 0.9	0.126	0.03	0.03	–0.03	0.005	0.005
OD 1.2	0.063	0.01	0.01	–0.02	0.004	0.004
dark	0	0.00	0.00	0.00	0.000	0.000

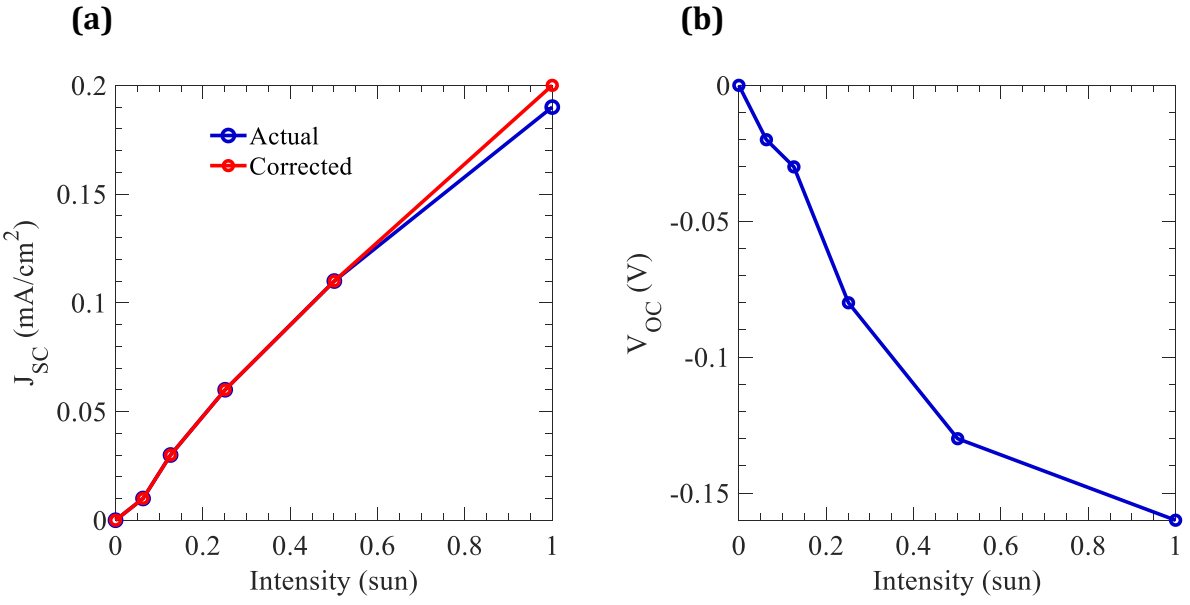

Figure 2.18: Fluence dependence of (a) actual and corrected J_{SC} and (b) V_{OC} values in the first batch of OsI_2 DSSCs where the calculated electrolyte solution potential is 0.29 V.

In addition to photoelectrochemical and fluence dependence measurements, ultraviolet–visible absorption spectroscopy was carried out for OsI_2 DSSCs before and after the photoelectrochemical measurements to measure the solar cell stability during the photoelectrochemical measurements.

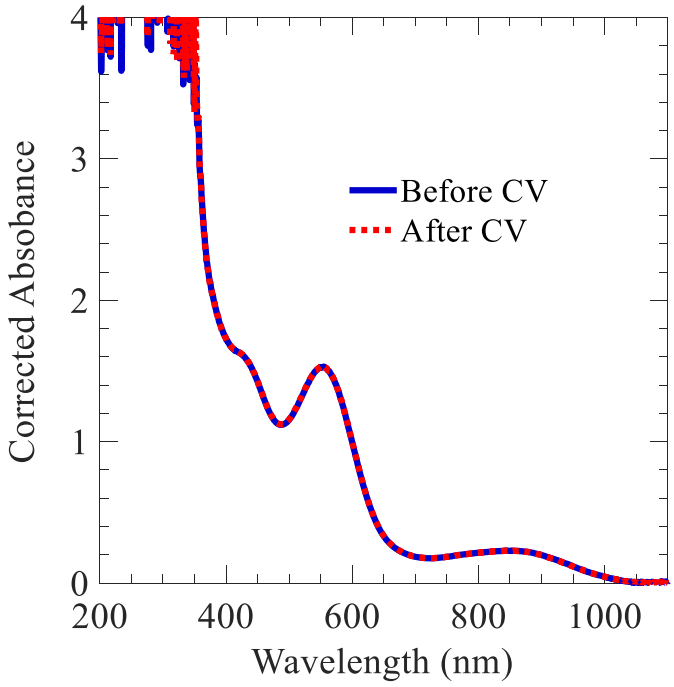

Figure 2.19: UV-Vis measurements performed before and after electrochemical measurements on the second batch of OsI_2 DSSCs at the spectra from 1100 to 200 nm.

The absorption spectra from 1100 to 200 nm demonstrate that all batches OsI_2 of DSSCs have the same absorption both before and after the photoelectrochemical mesurements. This indicates that no significant degradation of the dye or redox shuttle has occurred.

2.4 Conclusion

The potential of ten electrolyte solutions with distinct ratios of $[I^-]$ to $[I_3^-]$ were calculated using the Nernst equation. To ensure the solutions demonstrated the potentials obtained through calculations, their actual potential was measured by performing OCP and CV measurements with a potentiostat. The photoelectrochemical measurements show that the measured potential of electrolyte solutions is significantly different than the potentials obtained through calculations. One explanation for this difference is that in the calculation process it is considered that the electrolyte solution consists only I^- and I_3^- as the redox shuttle components and acetonitrile as the solvent. However, beside redox shuttle components and acetonitrile, the actual solution includes valeronitrile as the other solvent and trifluoroacetic acid and tetra-*n*-butylammonium perchlorate as the buffer components. The presence of the buffer components in the actual solution, and therefore H^+ ions, possibly degrade the performance of platinum working electrode.

Ten batches of RuN3 and OsI_2 DSSCs were fabricated with the same electrolyte compositions as those used for potential measurements. OCV, CV, and EIS measurements show that RuN3 DSSCs with the electrolyte in which the ratio of $[I^-]$ to $[I_3^-]$ is 6.335 are the most efficient. This is because their electrolyte is composed of enough I^- to quickly regenerate RuN3 dye and sufficient amount of I_3^- to quickly transfer electrons to the counter electrode. The fluence dependence measurements demonstrate that in both RuN3 and OsI_2 DSSCs, J_{SC} and light-to-electrical power conversion efficiency values increase almost linearly with increasing the incident light intensity, while the magnitudes of the V_{OC} values decrease nonlinearly. Though the ground-state reduction potential for oxidation of

the OsI_2 dye compared to the RuN3 dye is closer to the reduction potential of the redox shuttle, the power generated by OsI_2 DSSCs is insignificant and close to zero. The amount of power generated by these cells is very low most likely because kinetically the electron-transfer rate between the redox shuttle and OsI_2 is slow. Introduction of an electrocatalyst in the electrolyte solution of OsI_2 DSSCs may improve their performance.

Chapter 3

Foot-of-The-Wave Analysis

3.1 Introduction

The TiO_2 films that were used as a high band-gap semiconductor in the fabrication of DSSCs have a mesoporous geometry. Dye molecules bound to this mesoporous geometry exhibit non-ideal Nernstian redox behavior since in derivation of the Nernst equation, it is assumed that the molecules are moving freely in the solution and do not directly interact with each other, but, on a film, dyes are immobile and in intimately contact and/or directly interact with each other. Therefore, to study the catalysis behavior of a dye and the kinetics of charge-transfer between the bounded dye molecules and TiO_2 film, the Nernst non-ideality factor is introduced. To determine the Nernst non-ideality factor for $OsCl_2$ and OsI_2 dyes on a mesoporous TiO_2 film, potential-step chronoamperometry measurements were performed on $OsCl_2$ and OsI_2 dyed mesoporous TiO_2 working electrodes.

In this chapter, we are primarily interested in understanding how LiI and LiI_3, the components of the redox shuttle used in fabrication of RuN3 and OsI_2 DSSCs in Chapter 2, affect the amount of photocurrent produced by a working electrode. Furthermore, we want to determine if the addition of dmFc, a fast single-electron transfer reagent, to the electrolyte solution can improve the photocurrent. For this purpose, cyclic voltammetry measurements were performed on dyed TiO_2 working electrodes placed in an electrochemical beaker containing the supporting electrolyte solution and the substrate(s),

and the amount of current passed was measured as electric potential was varied. The consumption of the substrate(s) results in distortion of cyclic voltammetry responses at high current densities and overpotentials and this prevents extraction of kinetics information of the interaction between dyes and substrate under these conditions [23]. Foot-of-the wave analysis is a method that analyzes the cyclic voltammetry data in the "foot" region, meaning the very first points of the catalytic response, where the cyclic voltammetry responses are not affected by the perturbation caused by substrate consumption, inhibition by products, and IR drop [24]. The Nernst equation modified by the inclusion of a non-ideality factor is used in foot-of-the-wave analysis of cyclic voltammetry responses.

3.2 Experimental

3.2.1 Fabricating the Working Electrodes

For the purpose of spectroelectrochemical measurements and foot-of-the-wave analyses, we fabricated working electrodes according to the procedure explained in this subsection.

Glass Cutting and Labeling

To prepare the working electrodes, first 0.8 cm × 2.0 cm fluorine-doped tin oxide glass slides were cut with laboratory glass cutting table. A diamond tipped pen was used to label the slides on the non-conductive surface.

Glass Cleaning

To clean the slides of grease and most of other contaminants, they were sonicated in 5-10% wt aqueous Alconox solution for 15 min, rinsed with water and ethanol, and sonicated again for 15 min in ethanol. The slides were then rinsed with ethanol and allowed to dry. To burn off any remaining organic contaminant, they were heated to 550 °C on a hot plate for 1 h and then allowed to cool to room temperature.

TiO_2 Paste Application

After completing the cleaning process, TiO_2 paste was deposited on a narrow strip on the conductive side of FTO slide by the doctor-blade technique. Specifically, two parallel strips of Scotch 3M magic tape were placed on the conductive side of the slide, leaving a space about 0.5 cm between them near the bottom of the slide. A drop of the TiO_2 paste, which was also used for fabrication of DSSCs, was dripped on one edge of the slide between the two pieces of tape. A Teflon coated razor blade was used to spread the paste uniformly into a thin layer. The pieces of tape were removed carefully.

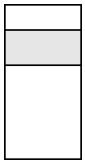

Figure 3.1: Doctor-blade location template for fabrication of working electrodes used in foot-of-the-wave analysis

Working Electrode Sintering

The slides were sintered in a muffle furnace first by heating at a rate of 180 °C/h to 90 °C, holding at that temperature for 1 h, then heating at a rate of 180 °C/h to 500 °C, and holding at 500 °C for 1 h. They were then allowed to cool to room temperature.

Working Electrode Assembly

A piece of insulated zinc-copper wire, stripped at both ends, with a total length of about 15 cm was attached to the other end of the conductive side of the working electrode. A copper foil tape with conductive adhesive (1", Freely Inc.) was used to attach the copper wire to the slide to make electrical contact between the wire and FTO. The copper tape and any exposed wire was then fully covered by a sealant silicone rubber (GE silicone II white bath caulk) and allowed to cure overnight. GE silicone II white bath caulk is resistant to methanol and acetonitrile (solvents in the dye solution) and is also an electrical insulator so it prevented electrochemical reactions between the copper tape and electrolyte solution during the measurements.

Dyeing Procedure

Before dying the working electrodes, the TiO_2 portion of each slide was immersed in a test tube filled with 1 mM tetra-*n*-butylammonium hydroxide solution for 15 min to improve the adsorption of dye molecules. The TiO_2 portion of each slide was immersed in water and acetonitrile respectively for 15 min in each. Then, to die the working electrodes, a 2 mM solution of dye in 1:1, v/v acetonitrile and methanol was prepared. There are two groups of working electrodes in this chapter which were fabricated with OsI_2 dye or with *cis*-$Os(dcbpy)_2Cl_2$ dye abbreviated as $OsCl_2$ (both synthesized by Joseph M Cardon, PhD candidate in Ardo Lab, UC Irvine). The TiO_2 portion of the working electrode was immersed in a test tube containing the die solution, the test tube was then sealed with parafilm so the solvents in the dye solution would not evaporate. Before doing any measurement, the

working electrode stayed overnight in a dye bath. Figure 3.2 (b) shows a sample of a fully fabricated $OsCl_2$ dyed working electrode.

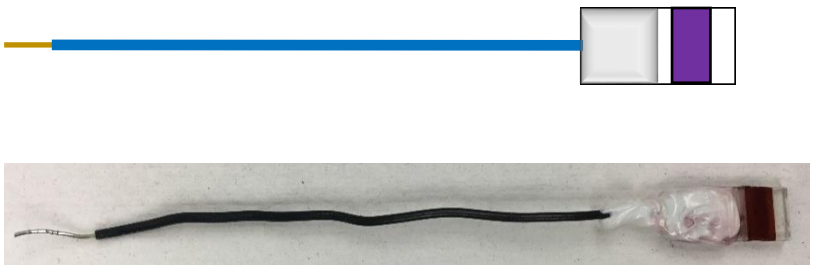

(a)

(b)

Figure 3.2: (a) schematic display of fabricated working electrode
(b) $OsCl_2$ dyed working electrode

3.2.2 Spectroelectrochemical Measurements of Dyed TiO_2 Films

Spectroelectrochemical measurements were used to determine the non-ideality factor (α) in the Nernst equation. Immediately prior to measurements, to remove weakly bound dyes, the dyed working electrodes were immersed in a test tube containing acetonitrile for 15 min and then they were immersed in fresh acetonitrile for another 15 min.

Experiment Setup

An aqueous KCl-saturated calomel electrode, a platinum mesh counter electrode and a fabricated dyed TiO_2 working electrode were used to perform three-electrode spcetroelectrochemical measurements. Initially, a 100 mM lithium perchlorate (battery grade 99.99%, Aldrich) in acetonitrile solution was prepared as a supporting electrolyte for the measurements. The three electrodes were placed in a spectroelectrochemical cuvette containing the supporting electrolyte. A rubber septum with three holes for the electrodes,

was placed over the cuvette to form an airtight seal. The cuvette was placed in the sample holder of a Cary 60 UV-Vis spectrophotometer and the three electrodes were connected to a Bio-Logic VSP-300 potentiostat with alligator clips. The position of the working electrode inside the cuvette was aligned so the dyed TiO_2 film was facing the incident beam to ensure it passed through the dyed area. Argon was bubbled through the solution during the measurement by a needle and another needle was used to vent the gas.

Preparing the UV-Vis Spectrophotometer

The absorption was measured using the instrument software with a 4800 nm min^{-1} scan rate and from 1100 to 200 nm wavelength. The baseline was set to *zero/baseline correction*. A blank measurement was collected through air and a dark measurement was collected by blocking the beam.

Rough E_0' Measurement

A 30-second OCP measurement was queued by setting all the limiting parameters to "pass" and the voltage range to 2.5 V. Then a cyclic voltammetry was queued with a scan rate of 50 mV s^{-1}, a starting potential of 0 V versus E_{OC} and the scan limits of –1 V and +1 V versus E_{OC}. The measurement was performed and the average of the forward and reverse duck peaks were taken, which is a rough approximation of E_0' for the system. The measured rough E_0' was consistently close to +0.23 V versus reference.

Nernst Non-ideality Factor Measurement

Initially, a 30-second OCP followed by a stepwise chronoamperometry measurements were queued for measurement by a potentiostat. To set the

chronoamperometry potential steps, the potential was stepped from 0.5 V negative of the measured E_0' to 0.5 V positive of E_0' with increments of 0.05 V, recording every 0.1 s for 30 min each. A prescan of the working electrode was taken using the UV-Vis spectrophotometer and the wavelength of the second peak (λ_{max}) was found. Kinetics measurement were subsequently performed by UV-Vis spectrophotometer at λ_{max} with a maximum scan length of 1 h. Chronoamperometry sequence began about 5 s after running the kinetics scan. For each potential step, when there was no significant change in the kinetics scan, kinetic acquisition was stopped, a full spectrum UV-Vis scan was done, a new kinetics scan was initiated, and next voltage step of chronoamperometry was started. This process typically took 5 to 15 min per step. The sequence of full spectrum scan, kinetics scan and chronoamperometry was repeated until all the potential steps were cycled through. The last voltage step reduced the dyed film again to check if any irreversible degradation had occurred and to prepare it for the next measurement.

3.2.3 Foot-of-the-Wave Analysis Measurement

Foot-of-the-wave analysis measurement was performed to study the catalytic effect of LiI, LiI_3, and 1,1′-Dimethylferrocene (97%, Alfa Aesar) on the performance of the fabricated working electrode.

Experiment Setup

A 10 mL acetonitrile solution containing 100 mM lithium perchlorate ($LiClO_4$) and 10 mM 1,1′-Dimethylferrocene (dmFc) was prepared and poured into an electrochemical beaker. Based on the substrate which to be tested, a 10 mL of acetonitrile solution

containing 100 mM LiI, 100 mM LiI_3, or 10 mM dmFc + 100 mM $LiClO_4$ was prepared in a different vial. Three holes were made in a rubber septum and dyed TiO_2 working electrode, platinum mesh counter electrode and SCE reference electrode passed through these holes. The electrodes were placed in the electrochemical beaker and the septum was placed over it to form an airtight seal. The electrodes were then connected to a potentiostat. The beaker was purged with argon gas at a slow rate during the measurement and a needle was used to vent the gas.

Electrochemical Measurements

A 30-second OCP measurement was performed to ensure the electrodes are connected to the potentiostat correctly. An initial EIS measurement was performed at a potential of 0 V versus E_{OC} and signal amplitude of 10 mV over a frequency range of 2 Hz to 7 MHz collecting six points per decade. CV measurements with scan rates of 0.1, 0.2, 0.5, 1, 2, 5, 10, and 20 V s^{-1} were performed. Each scan was repeated twice for a total of three times. For the experiments where LiI_3 was present in the solution, to reduce the LiI_3, the starting potential was +0.9 versus reference and the scan limits were set to –0.3 V and +0.9 V versus reference. For the rest of the experiments, the starting potential was set to –0.2 V versus reference and lower and upper scan limits were –0.2 V and +1.0 V versus reference. Finally, a second EIS measurement was performed with the same settings as the first EIS measurement.

Injections

After the first series of electrochemical measurements were completed, the substrate solution was injected at intervals to gradually increase the concentration of

substrate in the supporting electrolyte solution. Using a needle, the substrate solution was added to the electrochemical beaker in five steps. After each injection the electrochemical measurements were performed again. The total amount of the injected substrate was 0.101 mL, 0.204 mL, 0.526 mL, 1.111 mL, and 2.500 mL in the first, second, third, fourth, and fifth injection, respectively.

3.3 Results and Discussion

3.3.1 Nernst Non-ideality Factor

The dye molecules which are used as the light absorber in the working electrodes, are bounded to the mesoporous insulating surface of the TiO_2 thin film. The Nernst Equation which predicts the overall potential of an electrochemical cell or individual half reactions, is derived based on assumptions that are true for highly disperse molecules that diffuse freely in a solution. However, even on the hours timescale, surface-bound molecules do not diffuse freely and are in close contact with other surface-bound molecules. Thus, a non-ideality factor is introduced to modify the Nernst equation for surface-bound molecules. This modification helps us to analyze the data collected through electrochemical measurements and foot-of-the-wave analysis of the dyed TiO_2 working electrodes more accurately. Equation (3.1) shows the inclusion of α in the Nernst equation where Q is the ratio of reduced to oxidized dye.

$$E' = E_0' - \frac{\alpha RT}{zF}\ln(Q) \tag{3.1}$$

To obtain α in Equation (3.1), steady state spectroelectrochemical measurements of dyed films in the supporting electrolyte (100 mM $LiClO_4$ in acetonitrile) were performed by

potential step chronoamperometry. After each potential step, to ensure that the film had reached equilibrium at the applied potential, kinetics at λ_{max} were observed until there was no significant change. Full absorption spectra of the film were obtained after each kinetics measurement. The absorbance values at each applied potential were normalized and then averaged across the full spectrum of interest. Thereafter, they were plotted as a function of potential using OriginPro 2017 64 bit software. The resulted plot had a sigmoid shape which was fitted by the Boltzmann sigmoid function (3.2) and the values of fitting parameters for the plotted curve were extracted.

$$y = A_2 + \frac{A_1 - A_2}{1 - e^{\frac{x - x_0}{dx}}} \tag{3.2}$$

Each term of the Equation (3.2) can be translated into the physical values of the Nernst equation, such that A_1, A_2, x_0 and dx each translates as the normalized absorbance of fully reduced dye, the normalized absorbance of fully oxidized dye, the standard potential of the dye (E_0'), and $\frac{\alpha RT}{zF}$, respectively. By substituting these terms into the Equation (3.1), α is obtained.

The spectroelectrochemical measurements involved $OsCl_2$ dyed films were performed before foot-of-the-wave analysis measurements, while for OsI_2 dyed films they were performed after foot-of-the-wave analysis measurements. The supporting electrolyte for all the spectroelectrochemical measurements was 100 mM $LiClO_4$ in acetonitrile. As an example of spectroelectrochemical measurements, Figure 3.3 shows the absorbance spectra of $OsCl_2$ dye on the TiO_2 film obtained through potential step chronoamperometry and the resulted sigmoid curve of the average normalized absorbance as a function of applied potential. The measured Nernst non-ideality factor for $OsCl_2$ and OsI_2 dyes on the

TiO_2 film of the working electrodes are given in Table 3.1. Each working electrode was used for foot-of-the-wave analysis measurements testing different susbtrates.

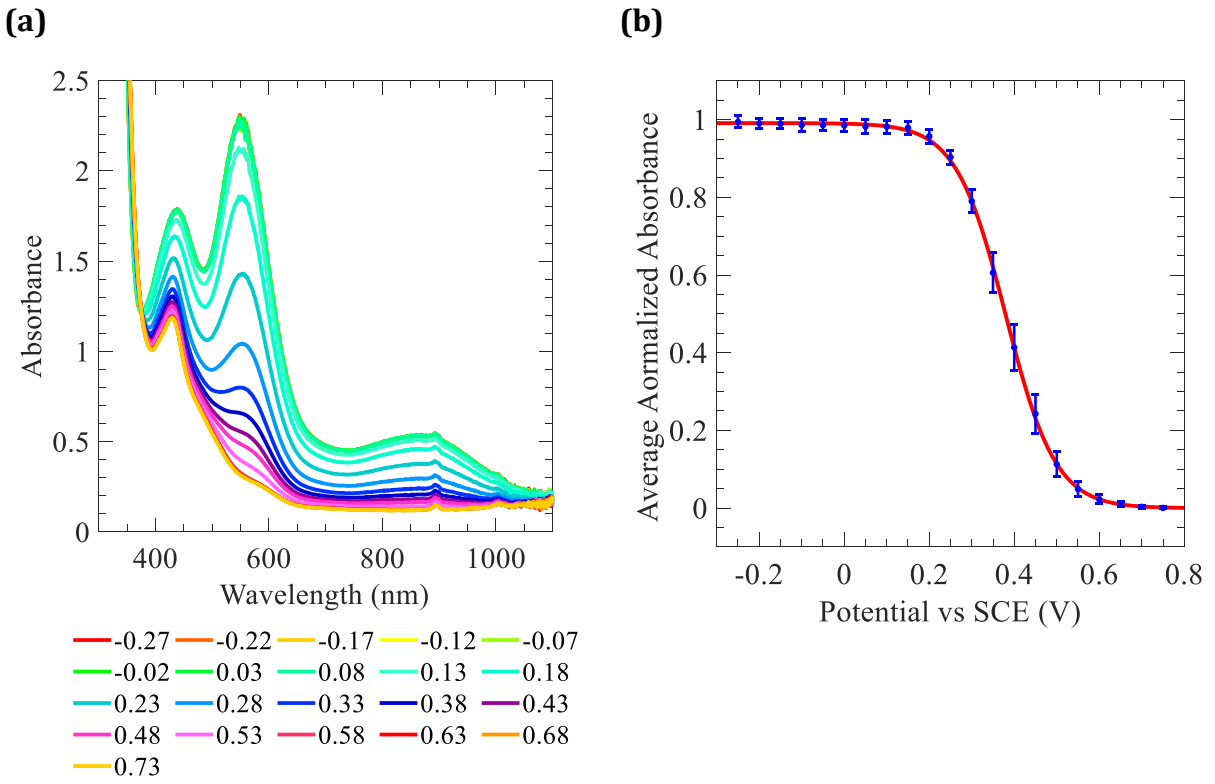

Figure 3.3: (a) Absorbance of $OsCl_2$ dye on the TiO_2 film over the range of 1100 to 200 nm at various applied potentials. The colors in the legend indicate applied potentials from –0.27 to 0.73 V versus SCE. (b) Average normalized absorbance as a function of applied potential fitted with the Boltzmann sigmoid function where error bars indicate one standard deviation.

Table 3.1: Nernst non-ideality factors for the $OsCl_2$ and OsI_2 dyes bounded to the TiO_2 film of the working electrodes which were used in foot-of-the-wave analysis measurements of different substrates.

Dye	Substrate(s)	α	Average α	Standard Deviation
$OsCl_2$	dmFc	2.15	2.89	0.74
	LiI_3	3.63		
OsI_2	dmFc	2.69	2.90	0.79
	LiI	3.13		
	LiI_3	1.11		
	dmFc+LiI, dmFc+LiI_3	2.88		

3.3.2 Foot-of-the-Wave Analysis of $OsCl_2$ Dye on a Mesoporous TiO_2 Film with One Substrate

As explained in the introduction of this chapter, foot-of-the-wave analysis was applied to cyclic voltammograms of $OsCl_2$ and OsI_2 dyed working electrodes to obtain more accurate responses by avoiding the distortions that occur at high currents. Since $OsCl_2$ is a more stable dye than OsI_2 during prolonged electrochemical measurements, foot-of-the-wave analysis was first applied to cyclic voltammograms of $OsCl_2$ working electrodes. The ground-state reduction potential to oxidize $OsCl_2$ is +0.19 V versus SCE and its optical bandgap is 1150 nm, which is equivalent to 1.08 eV. The results from these measurements were then used as a positive control measurement for foot-of-the-wave analysis of cyclic voltammograms of OsI_2 working electrodes. The substrates which were tested were dmFc and LiI_3. The electrochemical measurements and foot-of-the-wave analysis showed the

effect of these two substrates on the amount of the current passed by $OsCl_2$ working electrodes.

The supporting electrolyte was 100 mM $LiClO_4$ in acetonitrile solution and for the measurements which involved dmFc as a substrate, the concentration of dmFc in the solution was 0.1 mM, 0.2 mM, 0.5 mM, 1 mM, and 2 mM after the first, second, third, fourth, and fifth injections, respectively. The cyclic voltammograms and foot-of-the-wave analyses at the scan rate of 0.2 V s^{-1} are shown in Figure 3.4 and the results of the analyses are shown in Figure 3.5.

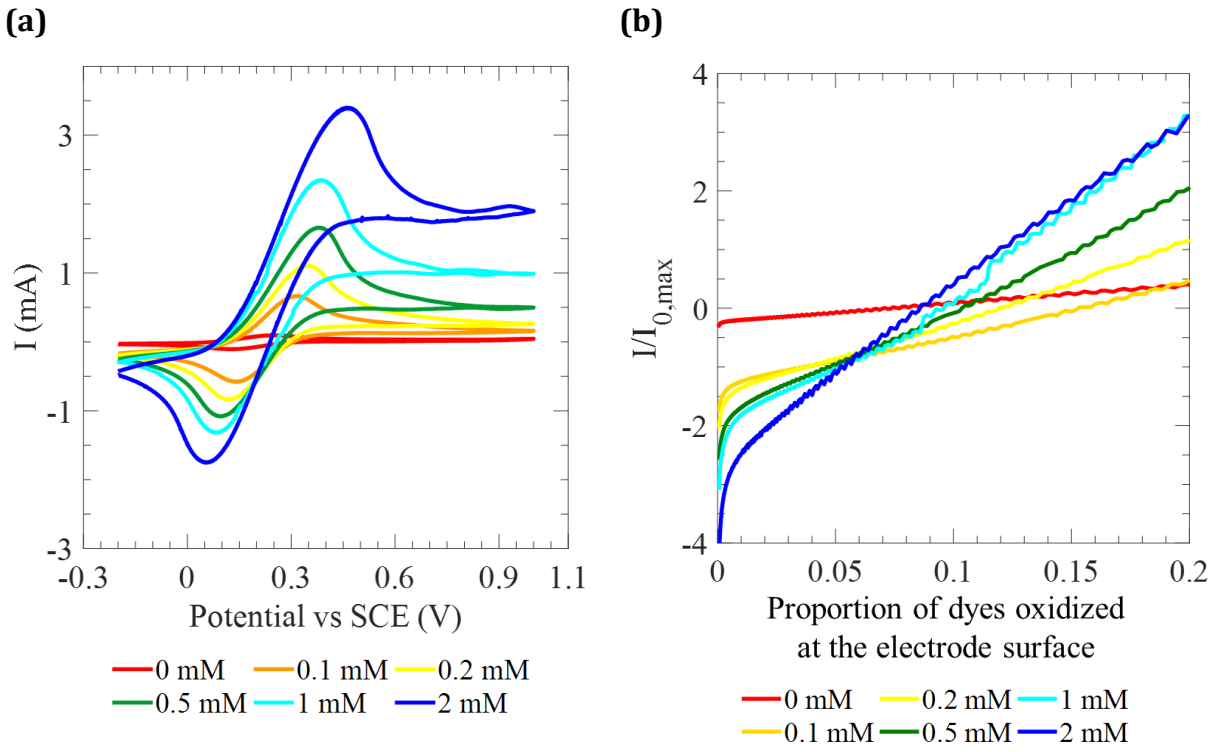

Figure 3.4: (a) Cyclic voltammograms of $OsCl_2$ dye on a mesoporous TiO_2 film at several concentartions of dmFc and the scan rate of 0.2 V s^{-1}. (b) Foot-of-the-wave (forward sweep) analyses of the cyclic voltammograms. The concentration of dmFc in 100 mM $LiClO_4$ in acetonitrile solution increases from 0 mM (red curves) to 2 mM (dark blue curves).

In Figure 3.4 (b), the current is normalized by the peak current with no added substrate and plotted versus the proportion of the dyes oxidized at the electrode surface. This ratio can be obtained from Equation (3.3) [23],

$$\text{Proportion of dyes oxidized at the electrode surface} = \frac{1}{1+\exp[\frac{-zF}{\alpha RT}(E'-E_0')]} \tag{3.3}$$

where α is the Nernst non-ideality factor, E' is the solution actual potential (V), E_0' is the solution potential at standard conditions (V), R is the universal gas constant (8.314472 J $K^{-1}mol^{-1}$), T is temperature (K), z is the number of electrons transferred in the cell reaction or half-reaction, and F is the Faraday constant (9.648533×10^4 C mol^{-1}).

Cyclic voltammograms in Figure 3.4 (a) show that the peak current increased when dmFc was added for both polarization directions, which is indicative of reversibility. Figure 3.4 (b) shows foot-of-the-wave curves for different concentrations of dmFc, where the

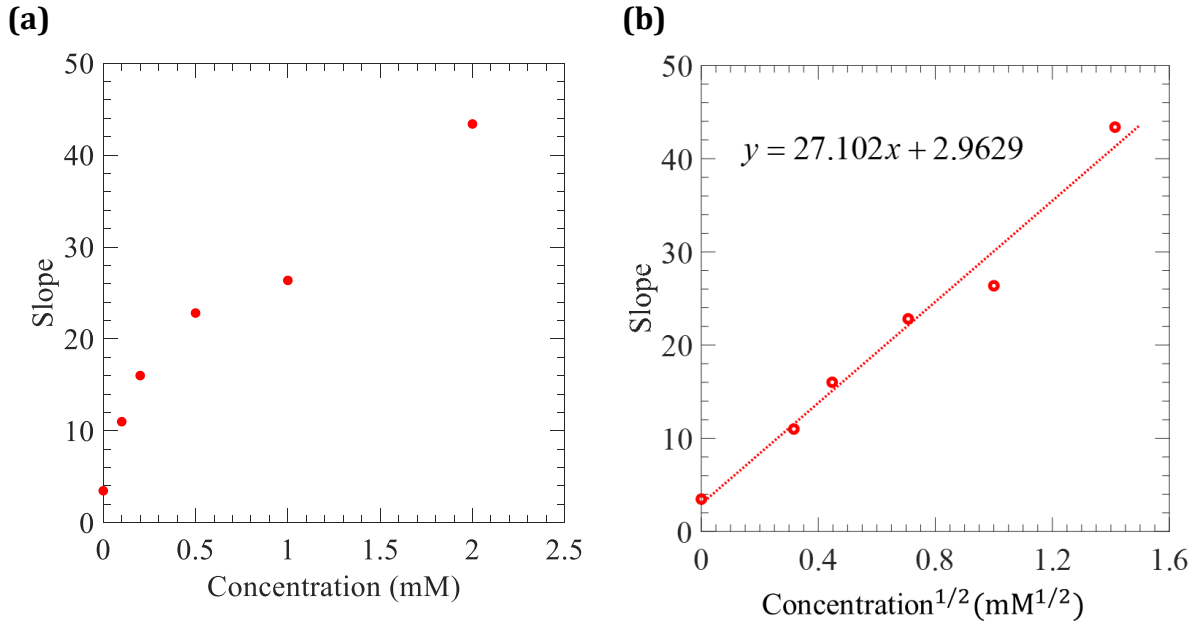

Figure 3.5: Foot-of-the-wave slope of $OsCl_2$ dye on a mesoporous TiO_2 film as a function of (a) concentration of dmFc (b) square root of concentration of dmFc at the scan rate of 0.2 V s^{-1}.

shape of the curves is nearly linear over the region shown with a slope that increases with concentration.

Figure 3.5 (a) shows the slope of the foot-of-the-wave data abstracted from the data in Figure 3.4 (b). The y values of Figure 3.5 (a) are important parameters because they contain the second-order rate constant. The slope is obtained using Equation (3.4) [23],

$$\text{Foot-of-the-wave slope} = 2.24\sqrt{\frac{RT}{F\nu}2k[substrate]} \qquad (3.4)$$

where R, T, and F are defined in Equation (3.3), ν is the scan rate (V s^{-1}), k is the fundamental charge transfer coefficient (M^{-1} s^{-1}), and $[substrate]$ is the concentration of the substrate (M). All the cyclic voltammograms and foot-of-the-wave curves in this chapter were obtained at the scan rate of 0.2 V s^{-1}. Figure 3.5 (a) illustrates that the slope icreases with increasing dmFc concentration. This shows that $OsCl_2$ does catalyze dmFc oxidation and the electron-transfer from dmFc to oxidize the dye is fast. Figure 3.5 (b) shows the slope as a function of square root of concentration of dmFc where based on Equation (3.4), the value of k can be extracted from the slope of linear trendline. The value of k for the electrochemical reaction between $OsCl_2$ and dmFc is $\sim 5.8 \times 10^5$ M^{-1} s^{-1}. A diffusion limited process would demonstrate a k value between 1×10^8 M^{-1} s^{-1} and 1×10^{10} M^{-1} s^{-1} depending on the size and diffusion coefficient of the species involved. This shows that the reaction of oxidized $OsCl_2$ dye with dmFc is not diffusion limited, but it is still considered fast by most standards.

Figure 3.6 illustrates the cyclic voltammograms and the corresponding foot-of-the-waves of $OsCl_2$ dyed working electrodes at the scan rate of 0.2 V s^{-1} where LiI_3 was used as a susbstrate in the supporting electrolyte solution. The concentration of LiI_3 in the solution

was 1 mM, 2 mM, 5 mM, 10 mM and 20 mM after the first, second, third, fourth and fifth injections, respectively. Figure 3.6 (a) shows that when LiI_3 was added the magnitude of the current increased only under the negative direction of polarization, which shows that catalysis only occurred for the reduction reaction. Figure 3.6 (b) is the foot-of-the-wave curves for different concentrations of LiI_3 and shows an increase in the slope by adding LiI_3. These two graphs are examples of foot of the wave analysis showing successful catalysis of only one direction of polarization. This occurs when the redox potential for the electrocatalyst is close to the potential of the reaction of interest.

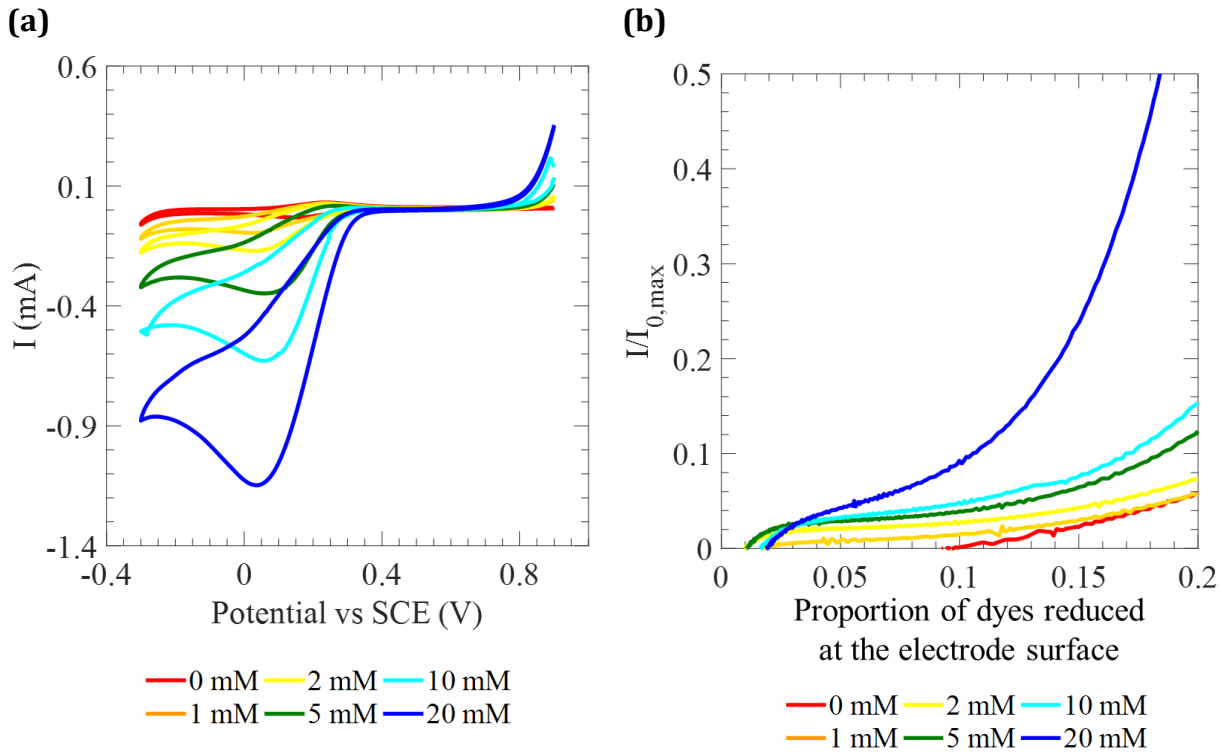

Figure 3.6: (a) Cyclic voltammograms of $OsCl_2$ dye on a mesoporous TiO_2 film at several concentartions of LiI_3 and the scan rate of 0.2 V s^{-1}. (b) Foot-of-the-wave (reverse sweep) analyses of the cyclic voltammograms. The concentration of LiI_3 in 100 mM $LiClO_4$ in acetonitrile solution increases from 0 mM (red curves) to 20 mM (dark blue curves).

Figure 3.7 illustrates that there is a slight enhancement of the slope by adding the LiI_3 substrate, where the magnitude of the slope changes from less than 0.5 to more than

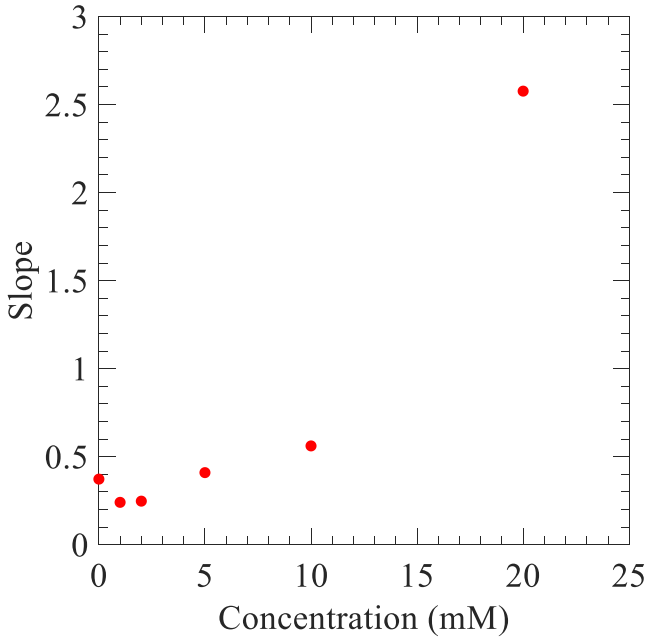

Figure 3.7: Foot-of-the-wave slope of $OsCl_2$ dye on a mesoporous TiO_2 film as a function of concentration of LiI_3 at the scan rate of 0.2 V s^{-1}.

2.5. It can be concluded that $OsCl_2$ does catalyze I_3^- reduction but the catalysis occurs slower than dmFc oxidation.

3.3.3 Foot-of-the-Wave Analysis of OsI_2 Dye on a Mesoporous TiO_2 Film with One Substrate

The results from foot-of-the-wave analyses of $OsCl_2$ dye on TiO_2 films with one substrate in the supporting electrolyte showed that this analysis is applicable to cyclic voltammetry catalytic responses of $OsCl_2$ dyes. At this stage, foot-of-the-wave analysis was adopted to analyze the data from the cyclic voltammetry measurements on OsI_2 dye which is analogous to $OsCl_2$ dye and is the dye that we used in fabrication of the second group of DSSCs in Chapter 2.

dmFc, LiI, and LiI_3 were the substrates used for electrochemical measurements of OsI_2 bound to TiO_2 working electrodes with one substrate. The supporting electrolyte for

all measurements was 100 mM $LiClO_4$ in acetonitrile solution. Figures 3.8 and 3.9 show the cyclic voltammograms and foot-of-the-wave analyses of OsI_2 working electrodes with dmFc at the scan rate of 0.2 V s^{-1}. The concentration of dmFc in the solution was 0.1 mM, 0.2 mM, 0.5 mM, 1 mM, and 2 mM after the first, second, third, fourth, and fifth injections, respectively.

The cyclic voltammetry measurements showed that increasing the concentration of dmFc from 0 mM to 2 mM in the electrolyte solution also increased the current. The cyclic voltammograms maintained almost the same shape as the substrate concentration increased (Figure 3.8 (a)). In Figure 3.8 (b) it is clearly shown that OsI_2 working electrode

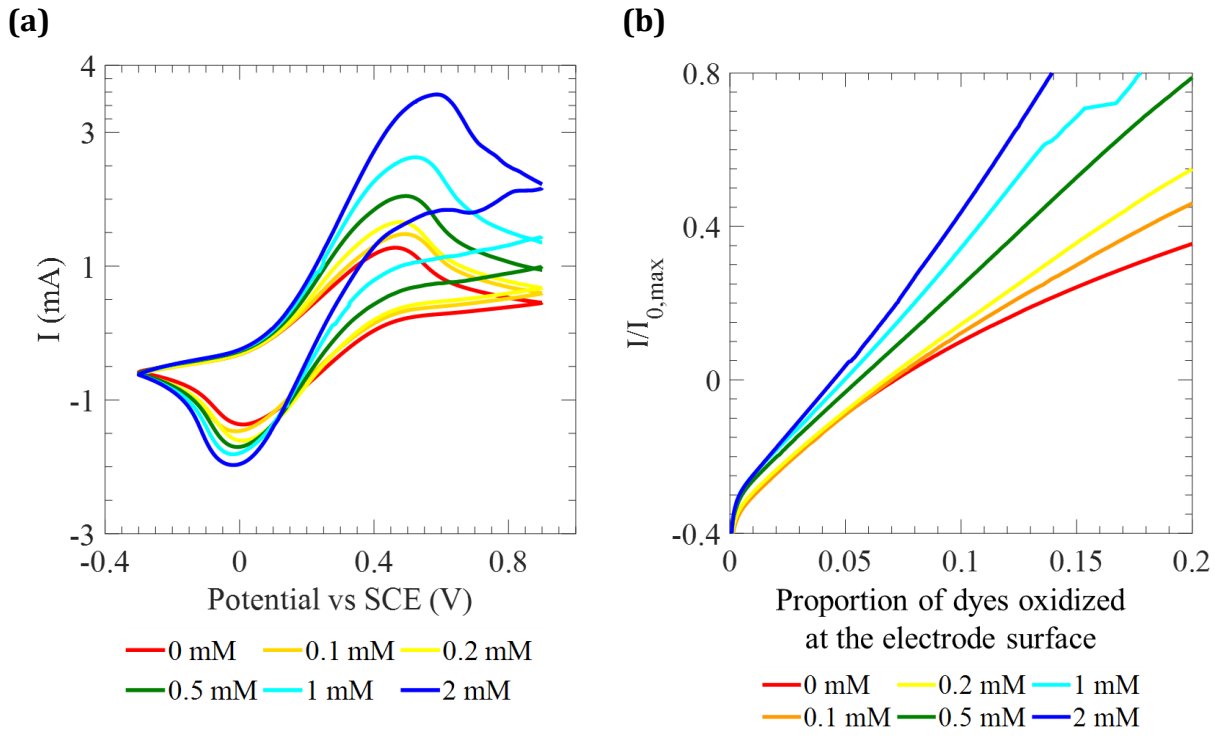

Figure 3.8: (a) Cyclic voltammograms of OsI_2 dye on a mesoporous TiO_2 film at several concentartions of dmFc and the scan rate of 0.2 V s^{-1}. (b) Foot-of-the-wave (forward sweep) analyses of the cyclic voltammograms. The concentration of dmFc in 100 mM $LiClO_4$ in acetonitrile solution increases from 0 mM (red curves) to 2 mM (dark blue curves).

generated more current by the addition of the substrate. It is observed that in Figure 3.9 (a) foot-of-the-wave slope increases linearly with increasing dmFc concentration which proves that OsI_2 does catalyze dmFc oxidation. The value of *k* for the electrochemical reaction between OsI_2 dye and dmFc is obtained from the slope of the linear trendline in Figure 3.9 (b) and it is $\sim 3.2 \times 10^3$ M^{-1} s^{-1} which is ~100 times slower than the fundamental charge transfer coefficient for the reaction between $OsCl_2$ and dmFc. This difference indicates that $OsCl_2$ is a better catalyst than OsI_2 for dmFc.

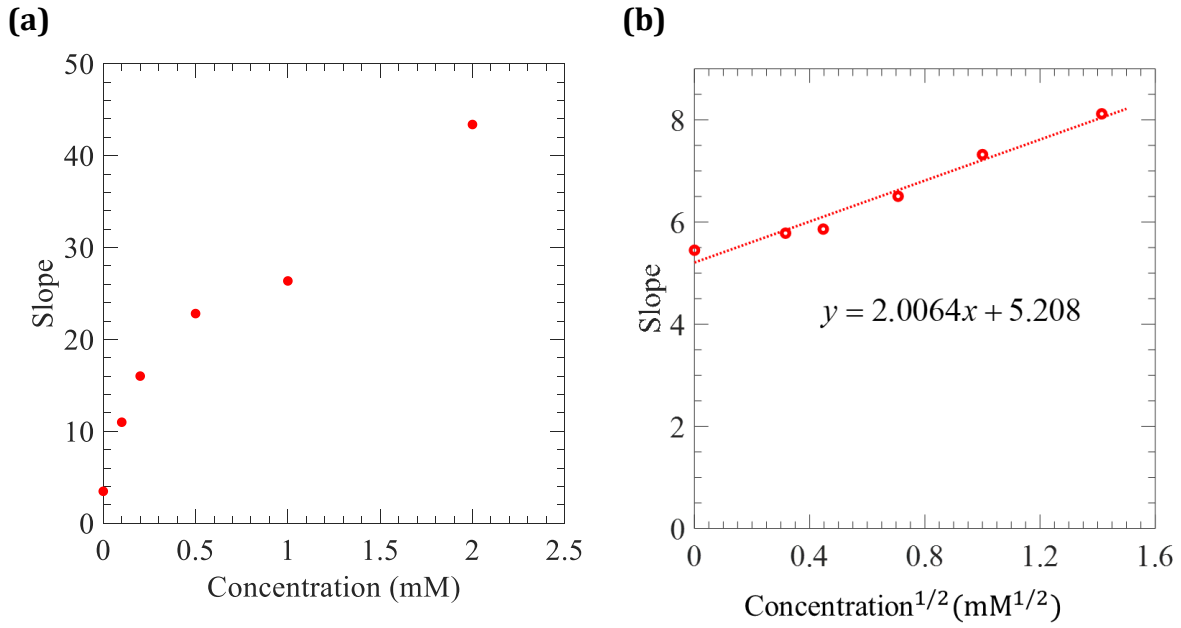

Figure 3.9: Foot-of-the-wave slope of OsI_2 dye on a mesoporous TiO_2 film as a function of (a) concentration of dmFc (b) square root of concentration of dmFc at the scan rate of 0.2 V s^{-1}.

LiI was used as the next substrate for foot-of-the-wave analysis of OsI_2 dye bound to a TiO_2 working electrode. The concentration of LiI in the supporting electrolyte solution was 1 mM, 2 mM, 5 mM, 10 mM, and 20 mM after the first, second, third, fourth, and fifth injections, respectively.

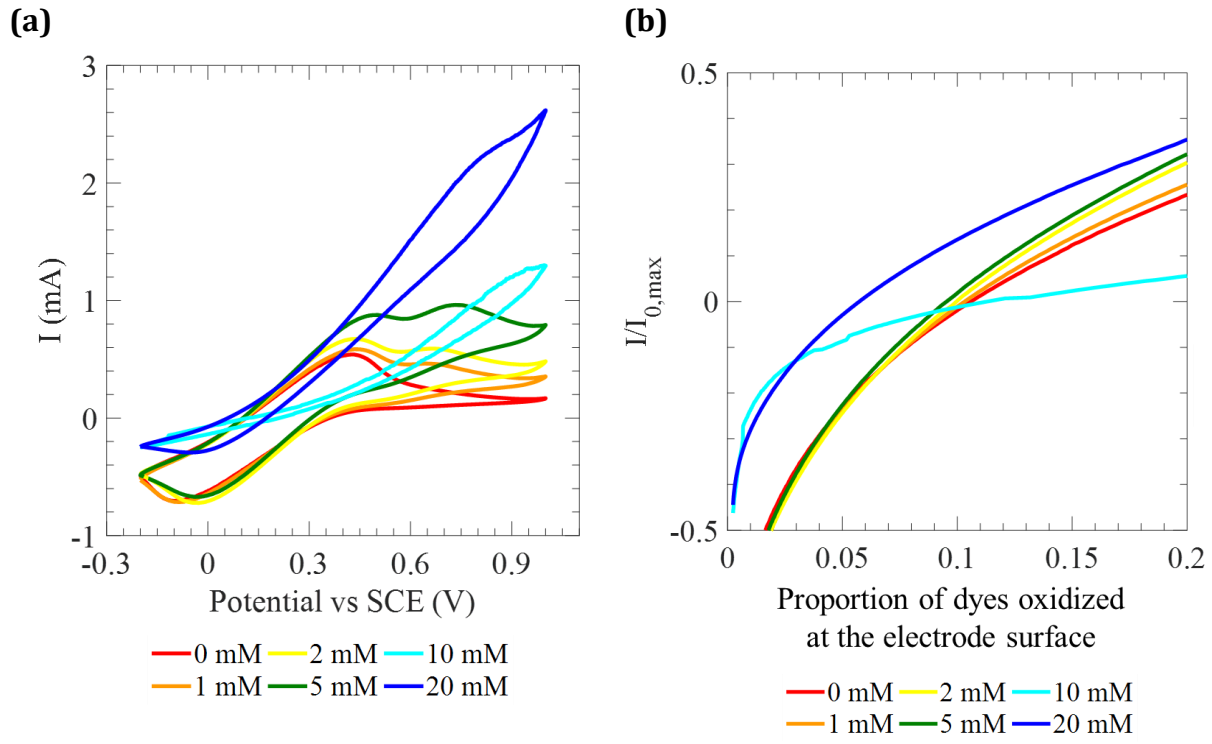

Figure 3.10: (a) Cyclic voltammograms of OsI_2 dye on a mesoporous TiO_2 film at several concentartions of LiI and the scan rate of 0.2 V s^{-1}. (b) Foot-of-the-wave (forward sweep) analyses of the cyclic voltammograms. The concentration of LiI in 100 mM $LiClO_4$ in acetonitrile solution increases from 0 mM (red curves) to 20 mM (dark blue curves).

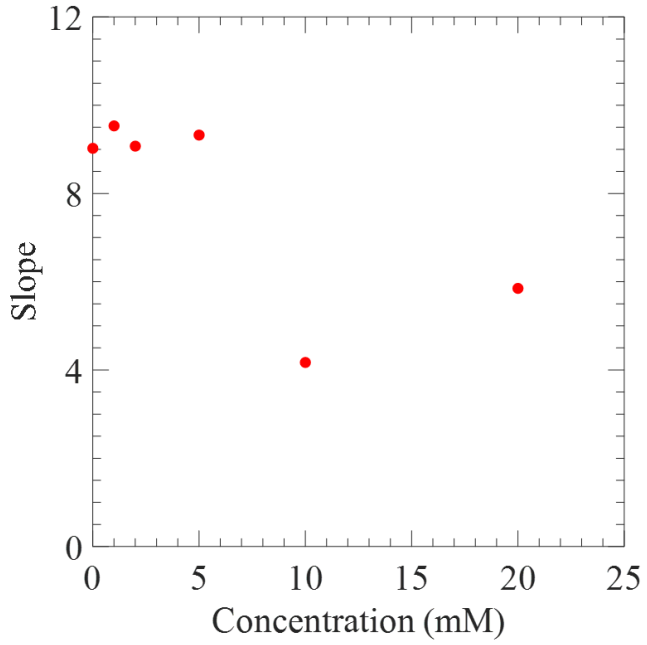

Figure 3.11: Foot-of-the-wave slope of OsI_2 dye on a mesoporous TiO_2 film as a function of concentration of LiI at the scan rate of 0.2 V s^{-1}.

The shape of the cyclic voltammograms of OsI_2 working electrode altered with increasing concentration of LiI and it is difficult to extract quantitative kinetics information from them. In Figure 3.10 (b), observation of the cyclic voltametry responses at low currents shows that except for 10 mM and 20 mM concentrations, the other traces overlap exactly, indicating no catalysis. In Figure 3.11 it is shown that there is no relationship between the slope of foot-of-the-wave curves and the concentration of LiI. This indicates that OsI_2 does not effectively catalyze I^- oxidation.

LiI_3 was the last substrate that was used in the series of cyclic voltammetry experiments and foot-of-the-wave analyses. Similar to LiI, the concentration of LiI_3 in the supporting electrolyte solution was 1 mM, 2 mM, 5 mM, 10 mM, and 20 mM after the first ,

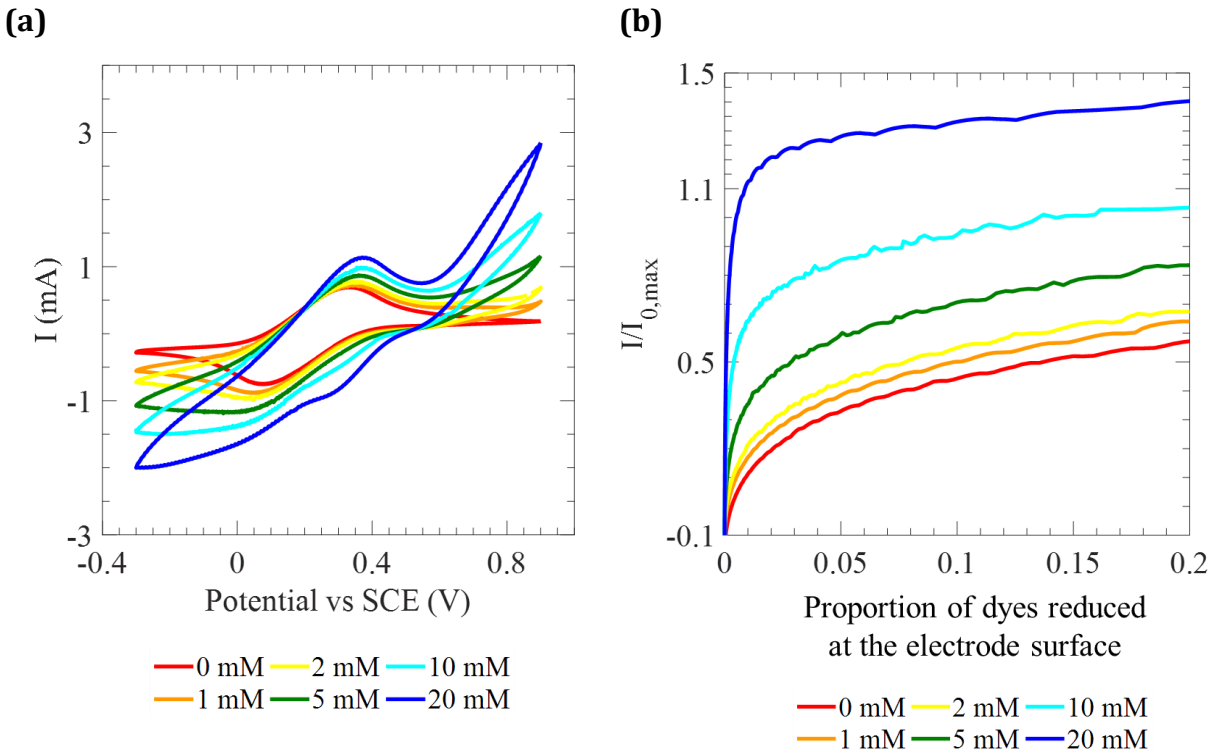

Figure 3.12: (a) Cyclic voltammograms of OsI_2 dye on a mesoporous TiO_2 film at several concentartions of LiI_3 and the scan rate of 0.2 V s^{-1}. (b) Foot-of-the-wave (reverse sweep) analyses of the cyclic voltammograms. The concentration of LiI_3 in 100 mM $LiClO_4$ in acetonitrile solution increases from 0 mM (red curves) to 20 mM (dark blue curves).

second, third, fourth, and fifth injections, respectively. In Figure 3.12 (b), foot-of-the-wave (reverse sweep) of cyclic voltammograms shows that there is no significant change in the slope of the curves at different concentrations of LiI_3. Figure 3.13 shows that there is an overall decrease in the foot-of-the-wave slope with increasing the concentration of substrate, which means that OsI_2 dye does not effectively catalyze I_3^- reduction.

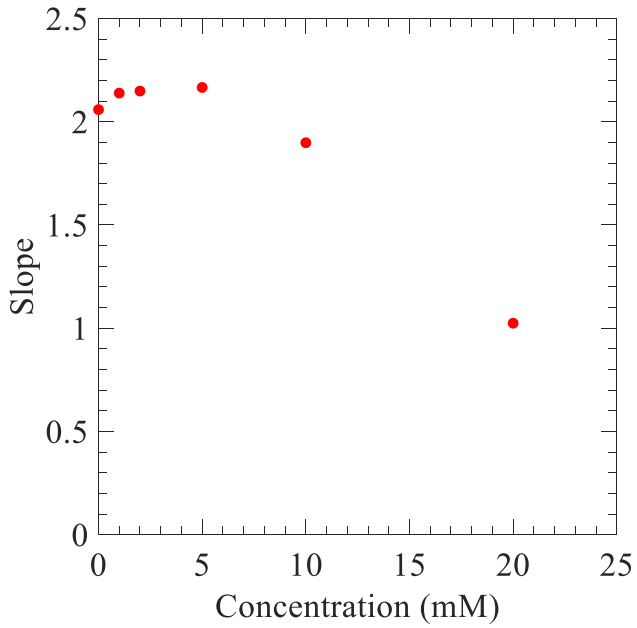

Figure 3.13: Foot-of-the-wave slope of OsI_2 dye on a mesoporous TiO_2 film as a function of concentration of LiI_3 at the scan rate of 0.2 V s^{-1}.

3.3.4 Foot-of-the-Wave Analysis of OsI_2 Dye on a Mesoporous TiO_2 Film with Two or More Substrates

The foot-of-the-wave analysis of OsI_2 dye on a mesoporous TiO_2 film with LiI as a substrate showed that OsI_2 does not effectively catalyze I^- oxidation. In this subsection we studied whether the addition of dmFc, which is a fast single-electron transfer reagent, can improve the rate of I^- electrocatalysis. Initially, electrochemical measurements and foot-of-the-wave analyses of OsI_2 working electrode in the presence of two substrates were

performed. The 100 mM $LiClO_4$ acetonitrile supporting electrolyte solution contained 10 mM dmFc while the concentration of the other substrate, LiI, was gradually increased by three injections. The concentration of LiI in the supporting electrolyte solution was 1 mM, 2 mM and 5 mM after the first, second and third injections, respectively.

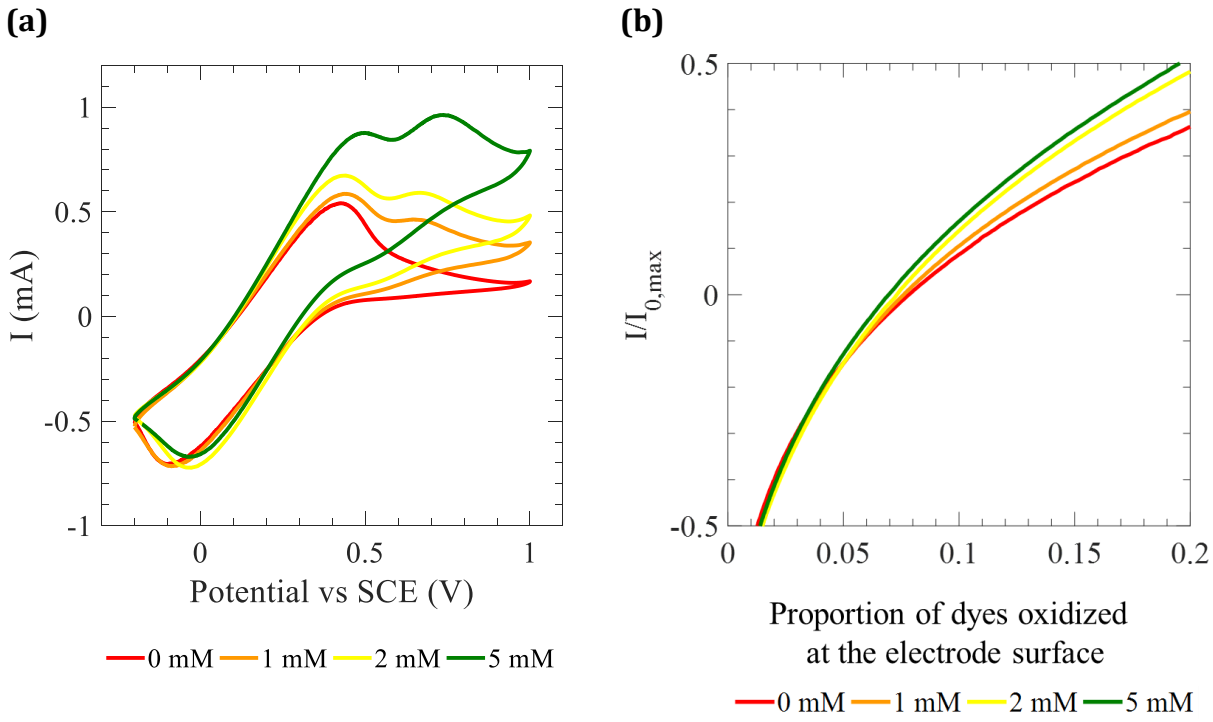

Figure 3.14: (a) Cyclic voltammograms of OsI_2 dye on a mesoporous TiO_2 film in the presence of 10 mM dmFc at several concentartions of LiI and the scan rate of 0.2 V s^{-1}. (b) Foot-of-the-wave (forward sweep) analyses of the cyclic voltammograms. The concentration of LiI in acetonitrile solution containing 100 mM $LiClO_4$ and 10mM dmFc increases from 0 mM (red curves) to 5 mM (green curves).

Foot-of-the-wave curves in Figure 3.14 (b) overlap each other almost perfectly and there is an insignificant increase in the amount of the normalized current upon increasing the concentration of LiI. This is also shown in Figure 3.15 where the foot-of-the-wave slope increases slightly from a less than 1.6 to 2.2 with increasing LiI concentration from 0 mM to 5 mM although the trend is monotonic. It can be interpreted that the addition of 10 mM dmFc to the electrolyte only slightly catalyzes I^- oxidation.

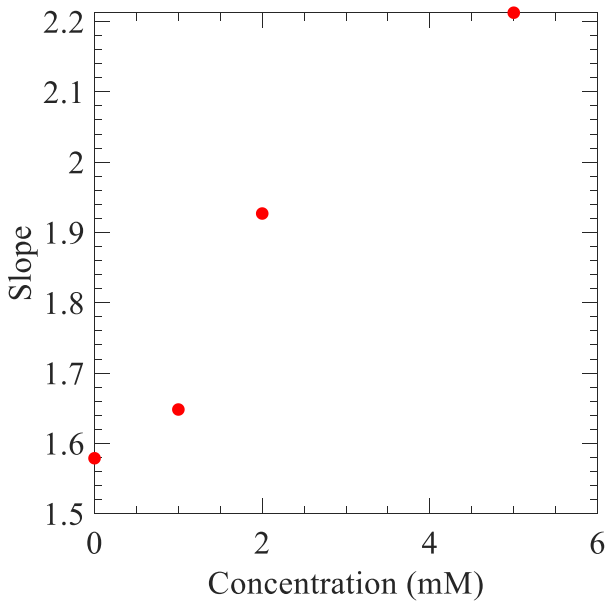

Figure 3.15: Foot-of-the-wave slope of OsI_2 dye on a mesoporous TiO_2 film as a function of concentration of LiI in the presence of 10 mM dmFc and at the scan rate of 0.2 V s^{-1}.

After the set of electrochemical measurements of OsI_2 working electrodes in the solution containing dmFc and LiI, it was desired to understand if the addition of dmFc affects the catalysis of LiI_3. Therefore, the electrochemical measurements and foot-of-the-wave analyses of OsI_2 working electrodes were performed in the presence of both dmFc and LiI_3. The concentration of dmFc in the supporting electrolyte solution was 10 mM and LiI_3 concentration in the solution was 1 mM, 2 mM and 5 mM after the first, second and third injections, respectively.

Figure 3.16 (a) shows that the cyclic voltammogram curves do not change drastically by increasing LiI_3 concentration. Foot-of-the-wave (backward sweep) curves in Figure 3.16 (b) are almost parallel to each other and according to Figure 3.17, there is no relationship between foot-of-the wave slope and the concentration of LiI_3. This implies that the addition of 10 mM dmFc to the electrolyte solution does not affect the the cataysis of LiI_3 and I_3^- is not effctively reduced.

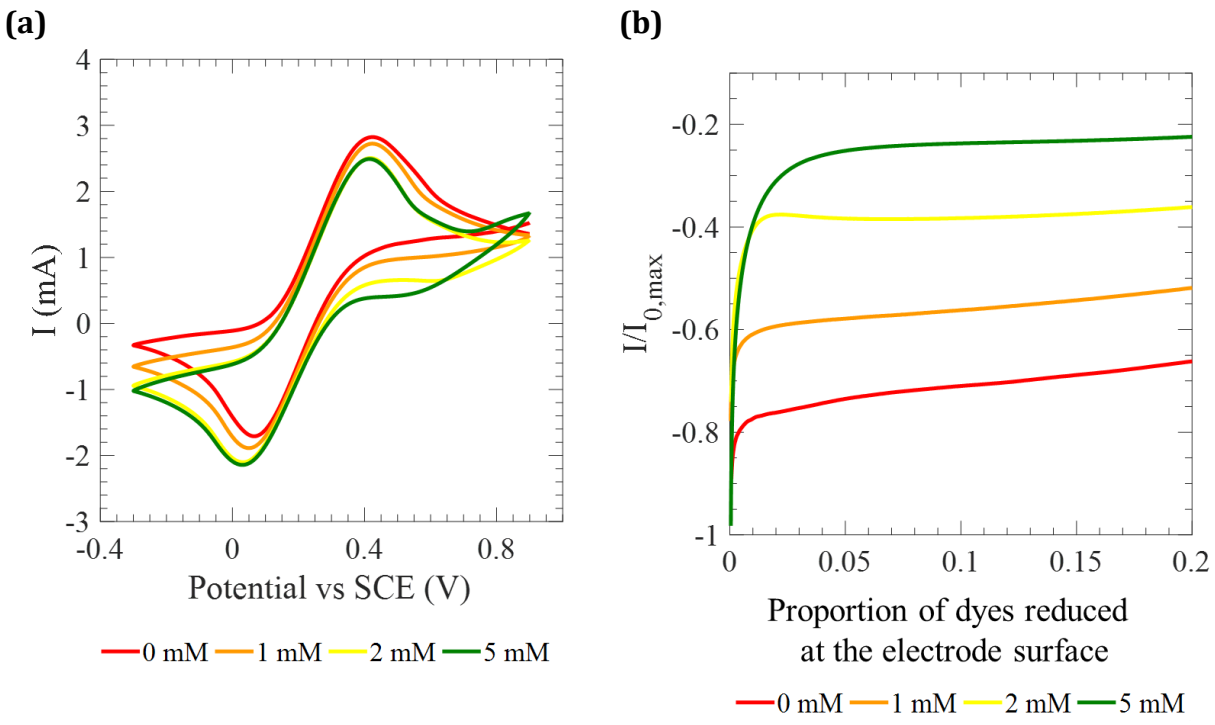

Figure 3.16: (a) Cyclic voltammograms of OsI_2 dye on a mesoporous TiO_2 film in the presence of 10 mM dmFc at several concentartions of LiI_3 and the scan rate of 0.2 V s^{-1}. (b) Foot-of-the-wave (reverse sweep) analyses of the cyclic voltammograms. The concentration of LiI_3 in acetonitrile solution containing 100 mM $LiClO_4$ and 10mM dmFc increases from 0 mM (red curves) to 5 mM (green curves).

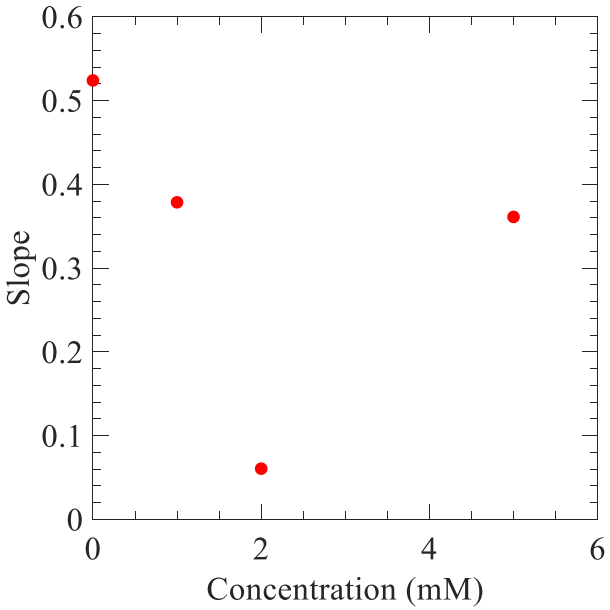

Figure 3.17: Foot-of-the-wave slope of OsI_2 dye on a mesoporous TiO_2 film as a function of concentration of LiI_3 in the presence of 10 mM dmFc and at the scan rate of 0.2 V s^{-1}.

At this stage, to simulate the OsI_2 DSSCs, which were fabricated and tested in Chapter 2, the electrolyte solution used in these solar cells was prepared and used as a substrate. However, to study the effect of dmFc on the catalysis of electrochemical reactions between I^- and I_3^-, the new electrolyte solution also included 10 mM dmFc. The concentrations of LiI and LiI_3 in the electrolyte solution were those which are mentioned in Table 2.4. Two sets of electrochemical measurements and foot-of-the-wave analyses of OsI_2 working electrodes were performed so that according to Table 2.4, in the first set the ratio

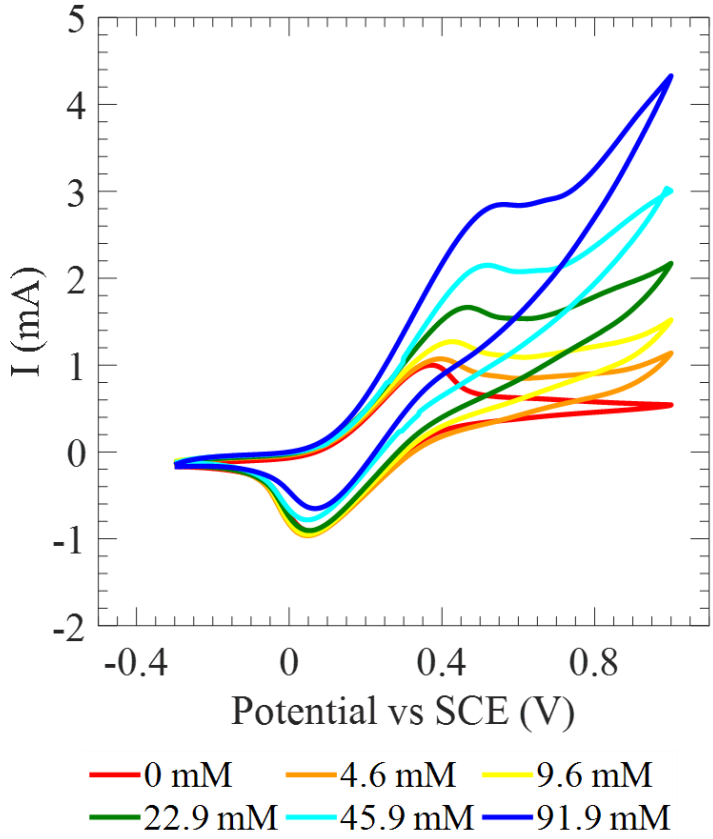

Figure 3.18: Cyclic voltammograms of OsI_2 dye on a mesoporous TiO_2 film at several concentartions of LiI and LiI_3 and the scan rate of 0.2 V s^{-1}. The ratio of $[I^-]$ to $[I_3^-]$ in the injections was 548.6. The concentration of LiI in the supporting electrolyte which was acetonitrile solution containing 100 mM $LiClO_4$ and 10mM dmFc increases from 0 mM (red curves) to 91.9 mM (dark blue curves).

of $[I^-]$ to $[I_3^-]$ in the electrolyte solution was 548.6 (similar to the first batch of OsI_2 DSSCs) and in the second set this ratio was 52.8 (similar to the second batch of OsI_2 DSSCs). The initial supporting electrolyte solution in the electrochemical beaker was acetonitrile solution containing 100 mM LiClO4 and 10mM dmFc.

In the first set of the measurements the concentration of LiI in the supporting electrolyte solution was 4.6 mM, 9.17 mM, 22.93 mM, 45.89 mM, and 91.8 mM after the first, second, third, fourth and fifth injections, respectively. For LiI_3, its concentration in the solution was 0.0083 mM, 0.0167 mM, 0.042 mM, 0.083 mM, and 0.167 mM after the first, second, third, fourth, and fifth injections, respectively. Figure 3.18 shows the cyclic voltammograms of OsI_2 working electrodes at several concentrations of the substrate which is the mixture of LiI, LiI_3 and dmFc. Since 10 mM of dmFc was already in the supporting electrolyte, presence of dmFc in the injections did not change its concentration significantly.

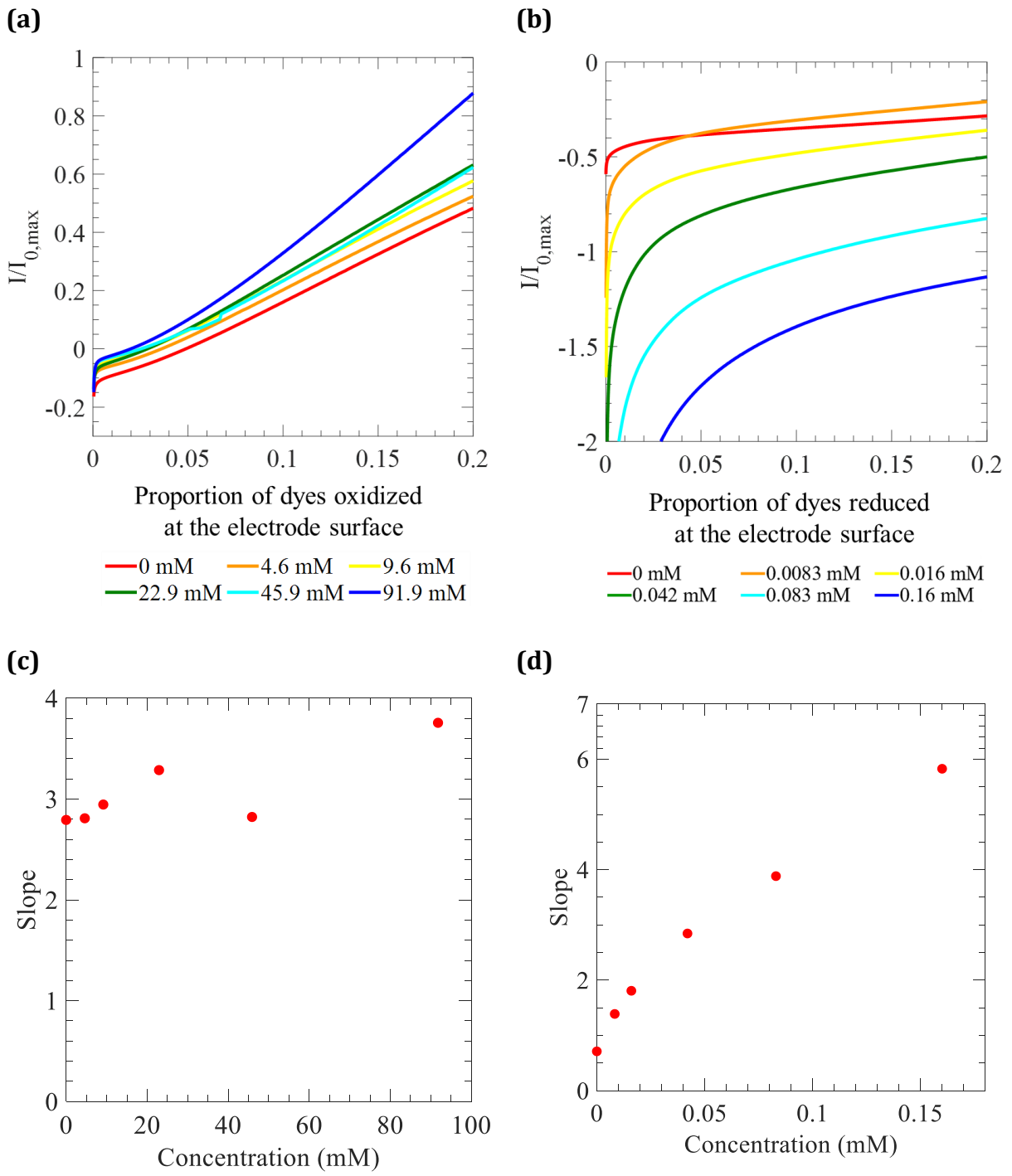

Figure 3.19: Foot-of-the-wave analyses of CV curves of OsI_2 dye on a mesoporous TiO_2 film at several concentartions of LiI and LiI_3 and the scan rate of 0.2 V s^{-1} when (a) the oxidation of I^- (forward sweep) and (b) the reduction of I_3^- (reverse sweep) is considered. Foot-of-the-wave slope as a function of (c) LiI concentration when the oxidation of I^-considered and (d) LiI_3 concentration when the reduction of I_3^- is considered. The ratio of $[I^-]$ to $[I_3^-]$ in the injections was 548.6.

Since the substrate includes both LiI and LiI_3, to better understand the catalysis effect of dmFc, foot-of-the-wave analyses were performed for oxidation of I^- and for reduction of I_3^-. Graphs (a) and (c) in Figure 3.19 show that dmFc in the presence of LiI and LiI_3 catalyzes the oxidation of I^- very slightly. On the other hand, it is clearly shown in Figure 3.19 (d) that foot-of-the-wave slope linearly increases by increasing the concentration of the LiI_3 in the solution. This indicates that dmFc catalyzes I_3^- reduction better than I^- oxidation under these conditions.

In the second set of electrochemical measurements and foot-of-the-wave analyses of OsI_2 working electrodes, the ratio of $[I^-]$ to $[I_3^-]$ in the injections was 52.770. The concentration of LiI in the supporting electrolyte solution was 4.5 mM, 9.0 mM, 22.53 mM,

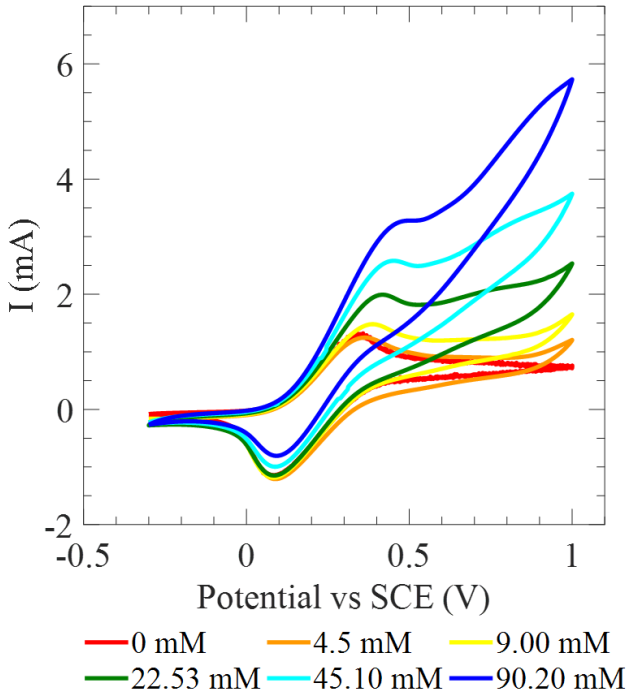

Figure 3.20: Cyclic voltammograms of OsI_2 dye on a mesoporous TiO_2 film at several concentartions of LiI and LiI_3 and the scan rate of 0.2 V s^{-1}. The ratio of $[I^-]$ to $[I_3^-]$ in the injections was 52.8. The concentration of LiI in the supporting electrolyte which was acetonitrile solution containing 100 mM $LiClO_4$ and 10mM dmFc increases from 0 mM (red curves) to 90.2 mM (dark blue curves).

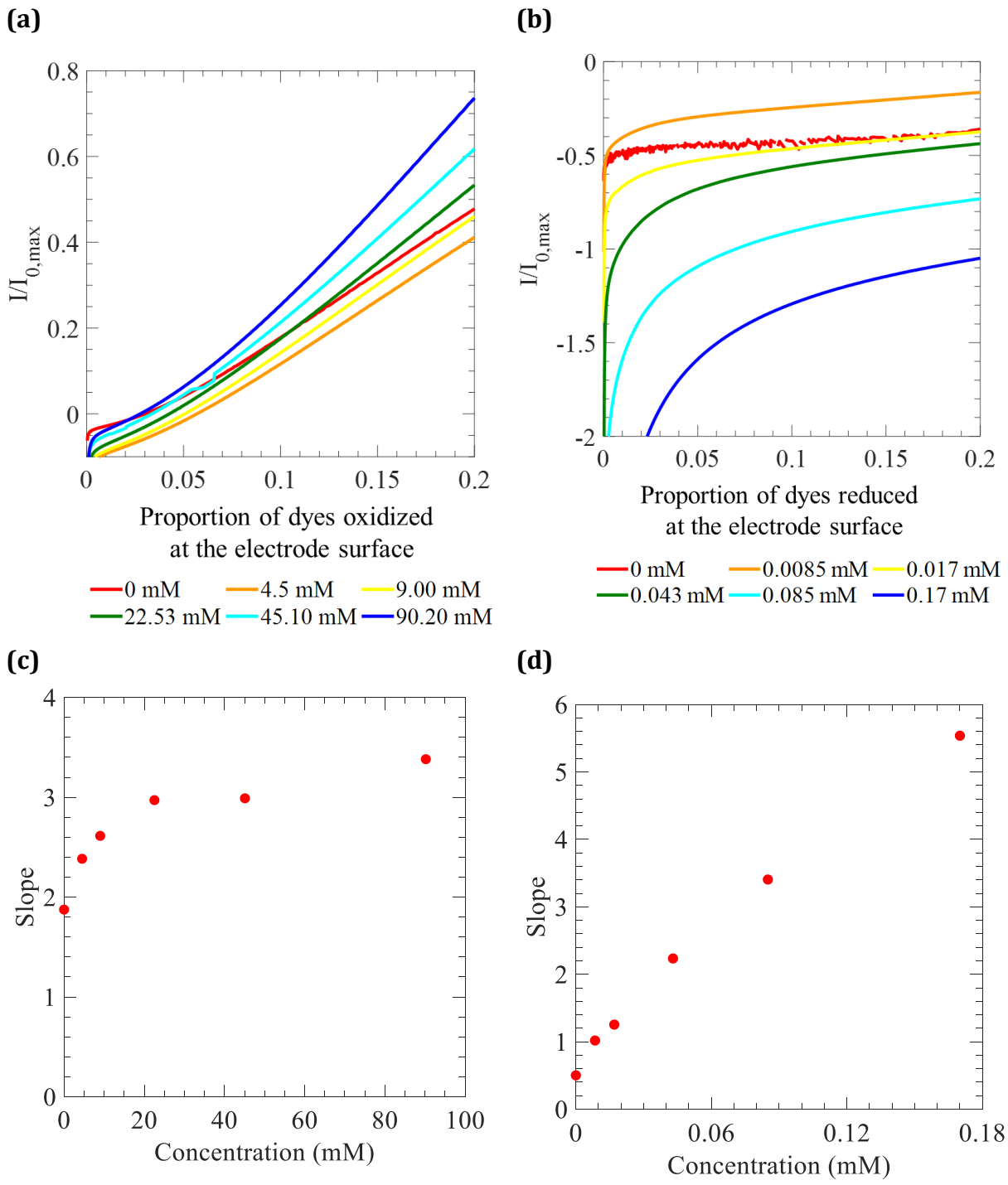

Figure 3.21: Foot-of-the-wave analyses of CV curves of OsI_2 dye on a mesoporous TiO_2 film at several concentartions of LiI and LiI_3 and the scan rate of 0.2 V s^{-1} when (a) the oxidation of I^- (forward sweep) and (b) the reduction of I_3^- (reverse sweep) is considered. Foot-of-the-wave slope as a function of (c) LiI concentration when the oxidation of I^-considered and (d) LiI_3 concentration when the reduction of I_3^- is considered. The ratio of $[I^-]$ to $[I_3^-]$ in the injections was 52.8.

45.10 mM, and 90.20 mM after the first, second, third, fourth, and fifth injections, respectively. For LiI_3, its concentration in the solution was 0.0085 mM, 0.0171 mM, 0.043 mM, 0.085 mM, and 0.171 mM after the first, second, third, fourth, and fifth injections, respectively. Similar to the first set of 3-substrate measurements results, foot-of-the-waves of cyclic voltammograms for the second set of measurements show that dmFc catalyzes both oxidation and reduction reactions; however, it catalyzes I_3^- reduction more than I^- oxidation. Figure 3.21 (c) shows that when the ratio of $[I^-]$ to $[I_3^-]$ in the injections decrease from 548.6 to 52.8 or in other words when the proportion of I^- in the solution increases, the oxidation of I^- by dmFc increases too.

3.4 Conclusion

Spectroelectrochemical measurements were performed to identify the Nernst non-ideality factor for oxidation of $OsCl_2$ and OsI_2 dyes on mesoporous TiO_2 film. $OsCl_2$ is a more stable dye compared to OsI_2. Therefore, spectroelectrochemical measurements were initially performed on $OsCl_2$ to use its results as a positive control measurement. The results showed that the mean non-ideality factor for $OsCl_2$ dyes bound to a TiO_2 thin film is 2.89 with the standard deviation of 0.74 and the mean non-ideality factor for OsI_2 dyes bound to a TiO_2 thin film is 2.90 with the standard deviation of 0.79. The obtained non-ideality factors were then used for calculation of the proportion of dyes oxidized or reduced at the electrode surface. This proportion is needed to produce accurate foot-of-the wave graphs.

To study the effect of dmFc on the catalysis of I^- oxidation and I_3^- reduction, a series of electrochemical measurements including OCP, EIS, and CV were performed. To avoid

distortion of cyclic voltammetry responses at high currents, foot-of-the-wave analysis of the cyclic voltammograms was performed which allowed us to extract kinetic information at lower currents. Foot-of-the-wave analyses of $OsCl_2$ working electrodes with one substrate demonstrated successful reversible catalysis of dmFc oxidation and successful one-direction catalysis of I_3^- reduction. It was shown that $OsCl_2$ does catalyze LiI_3 reduction but the catalysis occurs slower than dmFc oxidation. Foot-of-the-wave analyses of OsI_2 working electrodes with one substrate were then performed and showed that OsI_2 does catalyze dmFc oxidation. However, it does not effectively catalyze I^- oxidation and I_3^- reduction. Comparison between Figures 3.5 and 3.9 shows that the increase in foot-of-the-wave slope as a function of dmFc concentration, is much greater when $OsCl_2$ dye is used compared to when OsI_2 is used. This suggests that $OsCl_2$ dye is a much better catalyst than OsI_2 dye for oxidation of dmFc.

Foot-of-the-wave analyses of OsI_2 working electrodes with two substrates were performed in which one of the substrates, 10 mM dmFc, was present in the supporting electrolyte and the other substrate, LiI or LiI_3, was injected into the solution. It was shown that in the presence of dmFc, the oxidation of I^- is catalyzed very slowly and the reduction of I_3^- was not catalyzed. Then to simulate operating conditions of the first and second batch of OsI_2 DSSCs, the same electrolytes used in the solar cells, were fabricated with 10 mM dmF . The electrolytes with different ratios of $[I^-]$ to $[I_3^-]$ were injected into the initial electrolyte that also contained 10 mM dmFc. Foot-of-the-wave analyses of OsI_2 working electrodes with three substrates showed that in both of the measurements with $[I^-]$-to-$[I_3^-]$ ratios of 548.6 and 52.8, dmFc in the presence of LiI and LiI_3 mildly catalyzes both

oxidation and reduction reactions however, reduction of I_3^- is catalyzed more effectively than oxidation of I^-.

Chapter 4

DSSCs with Catalyst Additive

4.1 Introduction

In previous chapters OsI_2 was introduced as a dye with optical bandgap of 1050 nm, equivalent to 1.18 eV, which absorbs more infrared light compared to benchmark dye RuN3. It was predicted that DSSCs fabricated with OsI_2 would have higher efficiency than RuN3 DSSCs. However, results from photoelectrochemical measurements did not initially support this hypothesis and the amount of power generated by these solar cells was very low, most likely because the kinetics of electron transfer between the redox shuttle and OsI_2 is slow. The addition of an electrocatalyst to the electrolyte solution may speed up the electrochemical reactions and improve the overall performance of OsI_2 DSSCs. Foot-of-the-way analyses showed that the addition of dmFc to the electrolyte as a fast single-electron transfer reagent could modestly improve the kinetics of charge-transfer.

In Chapter 4, the electrocatalysis effect of dmFc on the performance of OsI_2 DSSCs is examined. For this purpose, two batches of OsI_2 DSSCs containing dmFc in their electrolyte solution were fabricated and tested. Similar to DSSCs without additives, the ratio of $[I^-]$ to $[I_3^-]$ in the two batches was varied. Two-electrode photoelectrochemical measurements including OCP, CV, an EIS were performed on these DSSCs using a solar simulator and a potentiostat to determine the J_{SC}, $V_{OC,}$ and light-to-electrical power conversion efficiency of the new OsI_2 DSSCs. The fluence dependence of solar cell performance was also tested by

using neutral density light filters during the photoelectrochemical measurements. Additionally, to measure the stability of solar cells during the photoelectrochemical measurements, UV-Vis spectroscopy was carried out before and after each photoelectrochemical measurement.

4.2 Experimental

The experimental sections of Chapter 2 and 4 are the same, except in Chapter 4 electrolyte solution preparation, the solution also included 10 mM dmFc. The rest of the section including preparation of DSSCs and measurement setups for photoelectrochemical characterization of DSSCs, fluence dependence, and UV-Vis spectroscopy are all the same.

4.3 Results and Discussion

4.3.1 Characterization of OsI_2 DSSCs containing dmFc

The third group of fabricated and characterized DDSCs incorporated the OsI_2 dye and dmFc as an electrocatalyst. Two batches of OsI_2 DSSCs with 10 mM dmFc in the electrolyte solution were fabricated so that the ratio of $[I^-]$ to $[I_3^-]$ in the first and second batch was 548.6 and 52.8, respectively. To understand how the addition of 10 mM dmFc to the electrolyte solution affects the performance of OsI_2 DSSCs, the solar cells were characterized by performing OCP, CV, and EIS measurements under illumination. The DSSC working and counter electrodes were connected to a Bio-Logic VSP-300 potentiostat and an initial OCP measurement was performed to ensure the solar cell was connected to the

potentiostat properly. The CV measurement was then performed to measure the current produced by the OsI_2 DSSC containing dmFc at potentials between 0.5 to –1.0 V. To measure the impedance of a solar cell and to find where it becomes fully real (Re(Z)), EIS measurement was performed at the frequency range of 1 kHz to 2 MHz. Three DSSCs were fabricated for both conditions to ensure the photoelectrochemical measurements results are reproducible.

Through the analysis of the photoelectrochemical measurement data, the critical parameters in characterizing a solar cell, J_{SC}, V_{OC} and light-to-electrical power conversion efficiency, were determined. Table 4.1 shows the values of these parameters for the two batches of OsI_2 DSSCs containing dmFc under 1 sun illumination intensity. Corrected J_{SC} and corrected efficiency values were calculated by mathematically correcting for resistive losses.

Table 4.1: The J_{SC}, V_{OC}, and efficiency values of OsI_2 DSSCs containing dmFc at two different electrolyte solution potentials under 1 sun illumination intensity.

	ratio of $[I^-]$ to $[I_3^-]$	measured electrolyte potential (V)	calculated electrolyte potential (V)	actual J_{SC} (mA cm^{-2})	corrected J_{SC} (mA cm^{-2})	V_{OC} (V)	actual efficiency (%)	corrected efficiency (%)
1	548.582	–0.0521	0.29	–0.05	–0.08	0.004	0.0002	0.0003
2	52.770	–0.0286	0.32	–0.06	–0.08	0.003	0.0002	0.0003

The very low values of J_{SC}, V_{OC} and efficiency presented in Table 4.1 do not confirm our hypothesis that the addition of dmFc to the electrolyte solution of OsI_2 DSSCs could improve their performance and result in higher amounts of power generation. Actual and corrected values for both J_{SC} and efficiency were nearly identical. However, it is interesting

to note the change of sign in J_{SC} and V_{OC} values compared to OsI_2 DSSCs without dmFc. The negative maximum current density and the positive maximum voltage are characteristic of a p-type solar cell. The results of photoelectrochemical measurements show that the fabricated OsI_2 DSSCs gained some p-type character at the presence of dmFc in its electrolyte solution. The TiO_2 semiconductor used in fabrication of OsI_2 DSSCs is an n-type semiconductor so it favors oxidation of dyes and redox electrolyte. However, the DSSCs acted as p-type solar cells which is backward of what we expected. A hypothesis to support this observation is that when dmFc is added to the electrolyte solution containing I^- and I_3^-, the electron-transfer direction changes and the electrons transfer from excited OsI_2 to the electrolyte solution instead of injecting from OsI_2 dye into the TiO_2 film. One possible mechanism is that an excited OsI_2 dye transfers an electron into $dmFc^+$ in solution faster than TiO_2, producing dmFc, which is capable of reducing I_3^- to I^- as shown in Chapter 3. Once this occurs, reduction of oxidized OsI_2 by I^- is slower than reduction of oxidized OsI_2 by thermally excited electrons in TiO_2 producing a net negative current. While this is interesting, the maximum light-to-electrical power conversion efficiency of a DSSC containing TiO_2 occurs when the reduction of dye sensitizers by I^- is fast, and the recombination kinetics between the injected electrons and I_3^- is slow [25]–[27].

Neutral density light filters were used during the photoelectrochemical measurements to study the effect of incident light intensity on the performance of OsI_2 DSSCs containing dmFc. Table 4.2 and Figure 4.1 show the results of fluence dependence measurement for the second batch of OsI_2 DSSCs containing dmFc where the ratio of $[I^-]$ to $[I_3^-]$ is 52.77. The maximum efficiency for both batches occurred at 0.063 sun intensity and the J_{CS} and V_{OC} values reached their maximum magnitude at 1 sun intensity. Figure 4.1

clearly demonstrates that unlike OsI_2 DSSCs without dmFc, the fluence dependence curves of OsI_2 DSSCs containing dmFc have a decreasing trend for J_{CS} and an increasing trend for V_{OC} with incresing the incident light intensity.

Table 4.2: Fluence dependence of J_{SC}, V_{OC} and efficiency values for the second batch of OsI_2 DSSCs containing dmFc where the potential of electrolyte solution is 0.32 V (calculated) and $[I^-]$-to-$[I_3^-]$ ratio is 52.770.

fluence	incident light intensity (sun)	actual J_{SC} (mA cm^{-2})	corrected J_{SC} (mA cm^{-2})	V_{OC} (V)	actual efficiency (%)	corrected efficiency (%)
no filter	1	−0.05	−0.08	0.004	0.0002	0.0003
OD 0.3	0.501	−0.03	−0.05	0.002	0.0003	0.0004
OD 0.6	0.251	−0.02	−0.03	0.001	0.0005	0.0006
OD 0.9	0.126	−0.01	−0.02	0.001	0.0007	0.0010
OD 1.2	0.063	0.00	−0.02	0.0003	0.0015	0.0021
dark	0	−0.01	−0.02	0.000	0.0001	0.0001

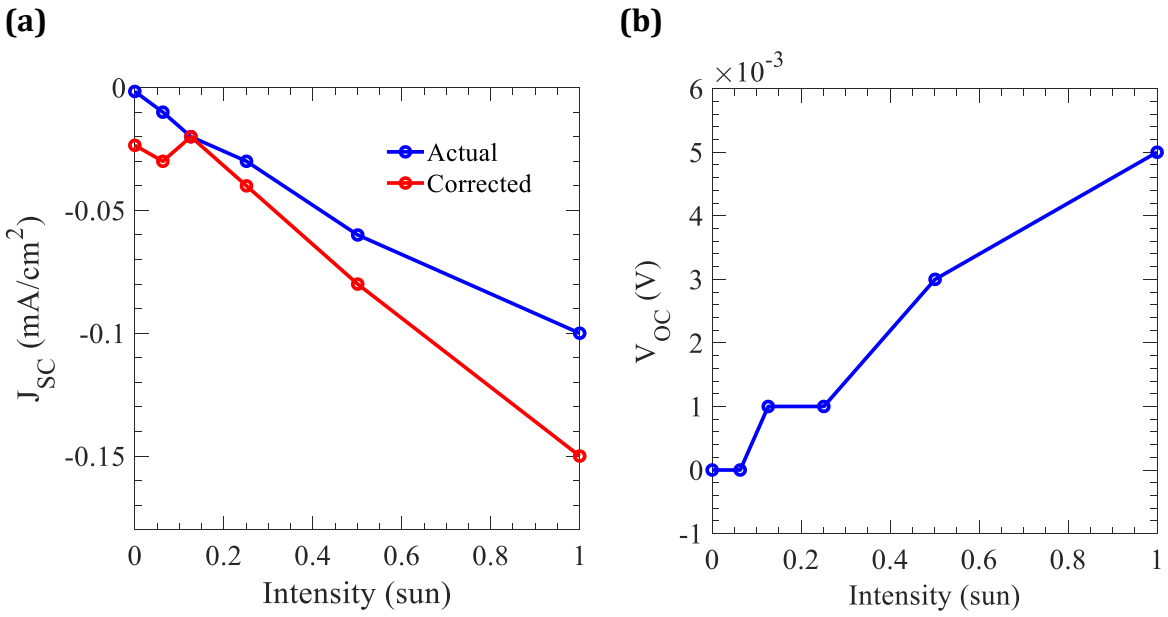

Figure 4.1: Fluence dependence of (a) actual and corrected J_{SC} and (b) V_{OC} values in the first batch of OsI_2 DSSCs containing dmFc where the calculated electrolyte solution potential is 0.29 V.

Ultraviolet–visible absorption spectroscopy from 1100 to 200 nm was carried out before and after the photoelectrochemical measurements. The purpose of this measurement was to study the stability of OsI_2 DSSCs containing dmFc during the photoelectrochemical measurements. Figure 4.2 shows the amount of light absorption at different wavelengths for one of the DSSCs from the second batch. The corrected absorbance curves obtained before and after the photoelectrochemical measurements at the selected spectra, almost perfectly overlap each other. Therefore, it can be concluded that the degradation of the dye or redox shuttle did not occur.

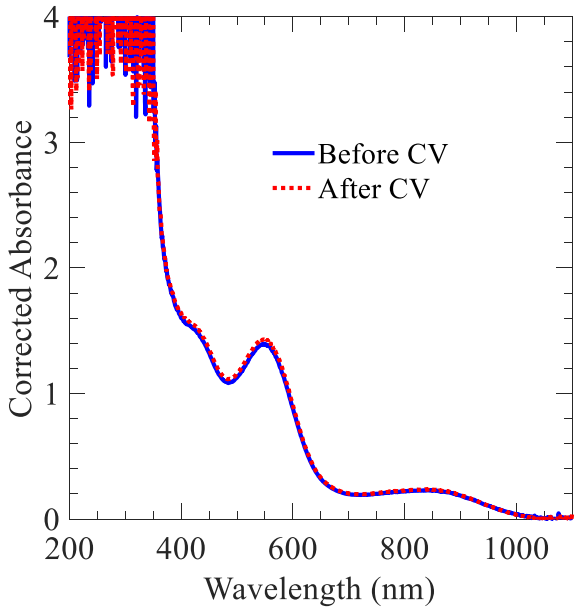

Figure 4.2: UV-Vis spectroscopy measurements performed before and after the photoelectrochemical measurements on one of the second batch OsI_2 DSSCs containing dmFc at the spectra from 1100 to 200 nm

4.4 Conclusion

To understand the role of dmFc on the charge-transfer rate at TiO_2-dye/electrolyte interfaces, two batches of OsI_2 DSSCs were fabricated with electrolyte solution containing

10 mM dmFc. The ratio of $[I^-]$ to $[I_3^-]$ was 548.6 and 52.8 in the first and second batch, respectively. The calculated electrolyte potential for the first batch was 0.29 V and for the second batch was 0.32 V. It was expected that addition of 10 mM dmFc would improve the slow kinetics of electrochemical reactions in OsI_2 DSSCs. However, the results of photoelectrochemical measurements including OCP, CV, and EIS did not meet our expectations and showed that the addition of dmFc to OsI_2 DSSCs not only did not improve the performance of these solar cells but surprisingly resulted in DSSCs that worked backward of what we expected. In other words, our OsI_2 DSSCs behaved as p-type solar cells even though they were fabricated with TiO_2, an n-type semiconductor which favors dye oxidation. A reason for this contradiction is that at the presence of dmFc, OsI_2 dye instead of injecting electrons to the TiO_2 film, injects them to the electrolyte solution, ultimately reducing I_3^-. This is consistent with foot-of-the-wave analyses results in Chapter 3 which showed that dmFc catalyzes the reduction of I_3^- faster than the oxidation of I^-. However, this finding while interesting, is not beneficial to maximizing efficiency because the maximum light-to-electrical power conversion efficiency of a DSSC containing TiO_2 occurs when the reduction of dye sensitizers by I^- is fast, and the recombination kinetics between the injected electrons and I_3^- is slow.

Fluence dependence measurements showed that the magnitudes of J_{SC} and V_{OC} of OsI_2 DSSCs containing dmFc increase with increasing the intensity of incident light and the maximum efficiency occurres at 0.063 sun intensity. Conducting ultraviolet–visible spectroscopy after and before the photoelectrochemical measurements demonstrated that at 1100 to 200 nm spectra, the OsI_2 dye or redox shuttle do not experience degradation during the photoelectrochemical measurements.

References

[1] M. A. Hasan and K. Sumathy, "Photovoltaic thermal module concepts and their performance analysis: A review," *Renew. Sustain. Energy Rev.*, vol. 14, no. 7, pp. 1845–1859, Sep. 2010.

[2] S. Fonash, *Solar Cell Device Physics*, 2 edition. Academic Press, 2010.

[3] M. K. Nazeeruddin, E. Baranoff, and M. Grätzel, "Dye-sensitized solar cells: A brief overview," *Sol. Energy*, vol. 85, no. 6, pp. 1172–1178, Jun. 2011.

[4] J. Gong, K. Sumathy, Q. Qiao, and Z. Zhou, "Review on dye-sensitized solar cells (DSSCs): Advanced techniques and research trends," *Renew. Sustain. Energy Rev.*, vol. 68, pp. 234–246, Feb. 2017.

[5] M. Grätzel, "Dye-sensitized solar cells," *J. Photochem. Photobiol. C Photochem. Rev.*, vol. 4, no. 2, pp. 145–153, Oct. 2003.

[6] B. O'Regan and M. Grätzel, "A low-cost, high-efficiency solar cell based on dye-sensitized colloidal TiO 2 films," *Nature*, vol. 353, no. 6346, p. 737, Oct. 1991.

[7] M. Ye *et al.*, "Recent advances in dye-sensitized solar cells: from photoanodes, sensitizers and electrolytes to counter electrodes," *Mater. Today*, vol. 18, no. 3, pp. 155–162, Apr. 2015.

[8] V. Sugathan, E. John, and K. Sudhakar, "Recent improvements in dye sensitized solar cells: A review," *Renew. Sustain. Energy Rev.*, vol. 52, pp. 54–64, Dec. 2015.

[9] J. Xu, K. Fan, W. Shi, K. Li, and T. Peng, "Application of ZnO micro-flowers as scattering layer for ZnO-based dye-sensitized solar cells with enhanced conversion efficiency," *Sol. Energy*, vol. 101, pp. 150–159, Mar. 2014.

[10] K. Song, I. Jang, D. Song, Y. S. Kang, and S.-G. Oh, "Echinoid-like particles with high surface area for dye-sensitized solar cells," *Sol. Energy*, vol. 105, pp. 218–224, Jul. 2014.

[11] M. R. Golobostanfard and H. Abdizadeh, "Hierarchical porous titania/carbon nanotube nanocomposite photoanode synthesized by controlled phase separation for dye sensitized solar cell," *Sol. Energy Mater. Sol. Cells*, vol. 120, pp. 295–302, Jan. 2014.

[12] X. Liu *et al.*, "Performance of four artificial chlorin-type sensitizers with different stereostructures in dye-sensitized solar cells," *Dyes Pigments*, vol. 98, no. 2, pp. 181–189, Aug. 2013.

[13] L. Wang *et al.*, "Influence of donor and bridge structure in D–A–π–A indoline dyes on the photovoltaic properties of dye-sensitized solar cells employing iodine/cobalt electrolyte," *Dyes Pigments*, vol. 101, pp. 270–279, Feb. 2014.

[14] M. Mao *et al.*, "Highly efficient light-harvesting boradiazaindacene sensitizers for dye-sensitized solar cells featuring phenothiazine donor antenna," *J. Power Sources*, vol. 268, pp. 965–976, Dec. 2014.

[15] J. Xia, F. Li, C. Huang, J. Zhai, and L. Jiang, "Improved stability quasi-solid-state dye-sensitized solar cell based on polyether framework gel electrolytes," *Sol. Energy Mater. Sol. Cells*, vol. 90, no. 7, pp. 944–952, May 2006.

[16] A. K. Arof *et al.*, "Efficiency enhancement by mixed cation effect in dye-sensitized solar cells with a PVdF based gel polymer electrolyte," *Int. J. Hydrog. Energy*, vol. 39, no. 6, pp. 2929–2935, Feb. 2014.

[17] L.-Y. Lin *et al.*, "A Low-Energy-Gap Organic Dye for High-Performance Small-Molecule Organic Solar Cells," *J. Am. Chem. Soc.*, vol. 133, no. 40, pp. 15822–15825, Oct. 2011.

[18] H. Liu, L. Liu, Y. Fu, E. Liu, and B. Xue, "Theoretical Design of D−π−A−A Sensitizers with Narrow Band Gap and Broad Spectral Response Based on Boron Dipyrromethene for Dye-Sensitized Solar Cells," *J. Chem. Inf. Model.*, Mar. 2019.

[19] S. Ahmad, E. Guillén, L. Kavan, M. Grätzel, and M. K. Nazeeruddin, "Metal free sensitizer and catalyst for dye sensitized solar cells," *Energy Environ. Sci.*, vol. 6, no. 12, pp. 3439–3466, Nov. 2013.

[20] S. Ito *et al.*, "Fabrication of thin film dye sensitized solar cells with solar to electric power conversion efficiency over 10%," *Thin Solid Films*, vol. 516, no. 14, pp. 4613–4619, May 2008.

[21] G. Boschloo and A. Hagfeldt, "Characteristics of the Iodide/Triiodide Redox Mediator in Dye-Sensitized Solar Cells," *Acc. Chem. Res.*, vol. 42, no. 11, pp. 1819–1826, Nov. 2009.

[22] S. Ching, R. Dudek, and E. Tabet, "Cyclic Voltammetry with Ultramicroelectrodes," *J. Chem. Educ.*, vol. 71, no. 7, p. 602, Jul. 1994.

[23] C. Costentin, S. Drouet, M. Robert, and J.-M. Savéant, "Turnover Numbers, Turnover Frequencies, and Overpotential in Molecular Catalysis of Electrochemical Reactions. Cyclic Voltammetry and Preparative-Scale Electrolysis," *J. Am. Chem. Soc.*, vol. 134, no. 27, pp. 11235–11242, Jul. 2012.

[24] D. J. Wasylenko, C. Rodríguez, M. L. Pegis, and J. M. Mayer, "Direct Comparison of Electrochemical and Spectrochemical Kinetics for Catalytic Oxygen Reduction," *J. Am. Chem. Soc.*, vol. 136, no. 36, pp. 12544–12547, Sep. 2014.

[25] S. Nakade, Y. Makimoto, W. Kubo, T. Kitamura, Y. Wada, and S. Yanagida, "Roles of Electrolytes on Charge Recombination in Dye-Sensitized TiO2 Solar Cells (2): The Case of Solar Cells Using Cobalt Complex Redox Couples," *J. Phys. Chem. B*, vol. 109, no. 8, pp. 3488–3493, Mar. 2005.

[26] A. Hagfeldt and M. Graetzel, “Light-Induced Redox Reactions in Nanocrystalline Systems,” *Chem. Rev.*, vol. 95, no. 1, pp. 49–68, Jan. 1995.

[27] I. Montanari, J. Nelson, and J. R. Durrant, “Iodide Electron Transfer Kinetics in Dye-Sensitized Nanocrystalline TiO2 Films,” *J. Phys. Chem. B*, vol. 106, no. 47, pp. 12203–12210, Nov. 2002.